AN ABSTRACT OF THE THESIS OF

Aaron M. Bevill for the degree of Master of Science in Nuclear Engineering presented on May 13, 2011.
Title: Performance of Hybrid Methods for Representative Nonproliferation Problems.

Abstract approved: _____

Todd S. Palmer

Adjoint-derived weight windowing is a hybrid deterministic/Monte Carlo method to simulate radiation transport. In adjoint-derived weight windowing, a deterministic adjoint solution is used to create weight windows for a Monte Carlo simulation. The intent of this work is to identify factors that reduce the Figure of Merit (FOM) of Monte Carlo simulations using adjoint derived weight windowing. The method used in this study pairs Transpire's deterministic code Attila^{TM} and MCNP5. Two computationally difficult source/detector problems of interest to nuclear nonproliferation are used as case studies to determine the factors that affect the FOM.

Test Case I is an active interrogation problem similar to many radiography problems. The model is used in two sets of trials: in the first, the quality of the deterministic adjoint solution is varied to observe the effect of adjoint solution quality on the FOM. In the second, the shielding density is varied to determine the effect of increased shielding on the FOM.

Results from Test Case I suggest that weight windows that decrease monotonically along relevant paths from the source to the detector maximize the FOM. The results also suggest that weight windowing is susceptible to false convergence that could be avoided using a different hybrid method, such as the Local Importance Function Transform (LIFT). A more sophisticated method for generating weight

windows relevant to the forward Monte Carlo simulation is described for future work.

Test Case II is a detailed model of a detector array passively interrogating a uranium hexafluoride cylinder. Test Case II is used to test the effect of appropriate source biasing on the FOM.

Results from Test Case II confirm prior work, that source biasing is important for problems in which the adjoint function varies widely in the source domain. Since spectral information from the detector is very useful for nonproliferation purposes, a new use of the forward weighted consistent adjoint driven importance sampling (FW-CADIS) method is described to model the energy-dependent flux in a region of interest. Properly modeling Test Case II also requires the use of rejection sampling of the source position paired with source biasing, which currently cannot be used together in MCNP5. The new use for the FW-CADIS method and a method to allow the use of rejection sampling with source biasing are described for future work.

Performance of Hybrid Methods for Representative Nonproliferation Problems

by

Aaron M. Bevill

A THESIS

submitted to

Oregon State University

in partial fulfillment of
the requirements for the
degree of

Master of Science

Presented May 13, 2011
Commencement June 2011

Master of Science thesis of Aaron M. Bevill presented on May 13, 2011.

APPROVED:

Major Professor, representing Nuclear Engineering

Head of the Department of Nuclear Engineering and Radiation Health Physics

---

Dean of the Graduate School

I understand that my thesis will become part of the permanent collection of Oregon State University libraries. My signature below authorizes release of my thesis to any reader upon request.

Aaron M. Bevill, Author

ACKNOWLEDGEMENTS

I would like to thank Dr. Todd Palmer for recruiting me to Oregon State University (OSU) and guiding my graduate career. He forced me to communicate my thoughts clearly and reconsider the best approach for difficult problems, all while offering me flexibility to pursue ideas tangentially related to my work. I would also like to thank him for introducing me to the field of hybrid methods and introducing me to our partners at Pacific Northwest National Laboratory (PNNL) and Dr. Ed Larsen at University of Michigan. I would like to thank Dr. Larsen, since his comments on adjoint-derived weight windowing and contributon flux in December of 2009 founded my conceptual understanding of hybrid methods.

I would like to thank Dr. Erin Miller (with whom I worked at PNNL) for her help in assembling the test problems and recommending a course of investigation. Special thanks is also owed to Matthew Gidden, Mark Shaver, and Dr. Eric Smith at PNNL for writing the template input deck for Test Case II.

I would like to thank the professors who taught courses that contributed to my understanding of numerical methods, including Dr. Jean Ragusa at Texas A&M University and Drs. Nathan Gibson, Todd Palmer, Brian Woods, Sourabh Apte, Guenter Schneider, and Alexey Soldatov at OSU.

I would like to thank the staff in the Nuclear Engineering / Radiation Health Physics Department at OSU, especially Kristie Marsh for her help navigating the graduation process. I would also like to thank Matthew Cleveland, Jacob Benz, and Brenton Ching, whose theses served as valuable references for form and styling.

Finally, I would like to thank my friends and family for their advise, suggestions, heckling, and support, including Nick (Nicky-D) Dorrell, Anh Mai, Mr. and

Dr. Ferguson, and Erica (Echo) Tobin. Special thanks go to Patrick and Terrie Bevill for pushing me through the last 22 years of toil and despair.

TABLE OF CONTENTS

Page

1 Introduction 1

1.1 Radiation Transport 2

1.1.1 The Steady-state Photon Transport 2
1.1.2 Numerical Methods for Solving the Transport Equation . . . 4

1.2 Monte Carlo Variance Reduction 5

1.3 Adjoint-Derived Weight Windows and Source Biasing 8

1.3.1 The Consistent Adjoint-Driven Importance Scheme 9
1.3.2 Forward Weighted CADIS 11

1.4 Source/Detector Approaches 11

1.5 Thesis Overview 12

2 Methods 15

2.1 Introduction 15

2.2 Deterministic Adjoint Solution 15

2.3 Creating Weight Windows 16

2.4 Source Biasing 17

2.4.1 Case I: Point Source 21
2.4.2 Case II: Volumetric Source 23

2.5 Monte Carlo 24

2.5.1 Monte Carlo Stopping Criteria 24
2.5.2 Post-Processing 25

3 Results 26

3.1 Introduction 26

3.2 Test Case I Description: Mulch Crate 26

TABLE OF CONTENTS (Continued)

Page

3.2.1 Test Case I Specifications: Attila™ 28
3.2.2 Test Case I Specifications: MCNP5 28
3.3 Test Case I Results 29
3.3.1 Effect of Adjoint Solution Quality on FOM 30
3.3.2 Effect of Shielding Density on FOM 30
3.4 Test Case II Description: Uranium Hexafluoride Cylinder 37
3.4.1 Test Case II Specifications: Attila™ 38
3.4.2 Test Case II MCNP5 Input 39
3.5 Test Case II Results 40
4 Conclusions 43
4.1 Introduction 43
4.2 Smoothness of Weight Windows 43
4.3 Advantage of CADIS 44
4.4 Comparison of Adjoint-Derived Weight Windowing with Alternative Methods 44
5 Future Work 47
5.1 Introduction 47
5.2 Use of FW-CADIS for Energy-Dependent Source-Detector Problems 48
5.3 An Improved Simplification Scheme for Weight Windows Generation 48
5.4 Extending the CADIS Source Distribution to Volumetric Sources in MCNP5 50

TABLE OF CONTENTS (Continued)

Page

Bibliography 52

Appendices 57

Appendix A Test Case I Specifications 58

Appendix B Test Case II Specifications 64

LIST OF FIGURES

Figure		Page
1	A slice of an example adjoint solution with ray effects perturbing the solution below 10^{-9} (light blue).	18
2	An example of data recorded in the search process used to find the ideal WGT parameter.	22
3	The top, front, and side views of the mulch crate model show Test Case I consists of a point source (sphere at left), shielding region, and detector region (cylinder at right).	27
4	A false-color plot of the deterministic adjoint flux solution at $z =$ 71.19 cm above the concrete slab with a mesh size of 15 cm.	32
5	A false-color plot of the deterministic adjoint flux solution at $z =$ 71.19 cm above the concrete slab with a mesh size of 30 cm.	33
6	A plot of the energy-dependent scalar adjoint flux solution along a line from the source ($\vec{x} =< -57.75, 0, 53.5 >$) to the detector ($\vec{x} =< 51.25, 0, 51 >$) with shielding density 0.5 g/cm^3.	35
7	A plot of the energy-dependent scalar adjoint flux solution along a line from the source ($\vec{x} =< -57.75, 0, 53.5 >$) to the detector ($\vec{x} =< 51.25, 0, 51 >$) with shielding density 2.0 g/cm^3.	36
8	A screenshot showing a large single-tally contribution to the detector between histories 49152000 and 57344000.	37
9	An isometric view of Test Case II shows the partly-filled UF_6 cylinder suspended above a "cart" and a large concrete slab.	38
10	The source biasing parameters as a function of x and y overlayed on a schematic showing the detector location in Test Case II.	41
11	In the distant interrogation problem, a neutron beam (green) is incident upon a target of interest (right).	49

LIST OF TABLES

Table		Page
1	Results from MCNP5 runs of the mulch problem at various mesh sizes after 600 minutes of simulation time	31
2	Results from MCNP5 runs of the mulch problem at various mulch densities	34
3	Details on the biasing parameters for Test Case II as a function of x, y, and z	40
4	Results from MCNP5 runs of Test Case II with various degrees of source biasing sophistication	41

LIST OF APPENDIX FIGURES

Figure		Page
12	The front view of Test Case II shows the large (diameter 76.2 cm) UF_6 cylinder, small cylindrical detector (at right), a metal slab representing a cart (center), and a large concrete slab (bottom).	64
13	The top view of Test Case II shows the large UF_6 cylinder and small detector suspended above the concrete slab.	65
14	The side view of Test Case II shows the small (diameter 12.7 cm) detector in front of the UF_6 cylinder.	66

LIST OF APPENDIX TABLES

Table		Page
5	Problem, mesh, cross section, source, and boundary value settings used in the deterministic simulation to generate adjoint flux moments	58
6	Quadrature, convergence, and output settings used in the deterministic simulation to generate adjoint flux moments	59
7	Extra reports used in the deterministic simulation gather information about the solution	60
8	Settings used in the report-only Attila™ simulation to generate weight windows from adjoint flux moments	61
9	Geometry input cards for the MCNP5 simulation used in the mulch case	61
10	Material compositions used in the MCNP5 model of the mulch case, expressed in weight percent	62
11	Histogram energy distribution for the mulch case	63
12	Problem, mesh, cross section, source and boundary value settings used in the Attila™ FSDS run to generate adjoint flux moments	67
13	Quadrature, convergence, and output settings used in the Attila™ FSDS run to generate adjoint flux moments	68
14	Settings used in the report-only Attila™ run to generate weight windows from adjoint flux moments	69
15	Cell input cards for the MCNP5 simulation used in Test Case II — detectors	70
16	Cell input cards for the MCNP5 simulation used in Test Case II — all geometry except detectors	71
17	Surface input cards for the MCNP5 simulation used in Test Case II — detectors	72
18	Surface input cards for the MCNP5 simulation used in Test Case II — all geometry except detectors	73
19	Material compositions used in the MCNP5 model of the UF_6 case, expressed in weight percent (or atom percent, as denoted by $^a/_0$)	74
20	Line energy spectrum of uranium-235 below 0.12 MeV	75
21	Line energy spectrum of uranium-235 above 0.12 MeV	76

Performance of Hybrid Methods for Representative Nonproliferation Problems

1 Introduction

Nuclear nonproliferation experts aim to prevent the spread of nuclear weapons, often by controlling and tracking the spread of certain radioactive materials. Radiation detectors — systems that electronically respond to the presence of radiation — can be used in several ways to quickly identify smuggled contraband: at ports and other critical gateways, hand-held and portal radiation detectors allow security officers to assess the quantity and type of nuclear material entering the country. In nuclear facilities abroad, cleverly placed detectors can quickly provide information about radioactive materials used in the plant without interrupting the facility. Outside of nuclear nonproliferation, X-ray radiography is commonly used to scan packages as small as passenger luggage and as large as containerized cargo on trucks [Miller 2010].

Radiation transport simulation — the study of radiation as it moves through matter — is important in nonproliferation for several reasons. Radiography and passive assay have vulnerabilities that reduce their sensitivity, such as the presence of shielding or intense background sources, that can be quickly assessed using simulation. New detection methods and equipment are often tested less expensively with simulation than experiment. Finally, an efficient transport simulation allows inverse problems, such as source location, to be solved in a timely manner. All three of these source/detector problems call for efficient photon simulation. This thesis focuses on the use of weight windowing to improve the efficiency of Monte Carlo simulation of photons in source/detector problems.

This chapter overviews the theory and previous work related to the topic of this thesis. Section 1.1 discusses radiation transport concepts, including relevant alternative representations that offer information about the region of interest as well as the source. Section 1.2 discusses variance reduction methods that have been used with Monte Carlo simulation. Section 1.3 specifically explores the use of adjoint-derived weight windows, including the use of source biasing to improve the efficiency of source sampling. Section 1.4 returns to the issue of source/detector problems, reviewing the use of adjoint-derived weight windows for problems with small regions of interest. Finally, Section 1.5 briefly overviews the remaining chapters in this thesis.

1.1 Radiation Transport

Radiation transport theory is the study of the distribution of radiation quanta as a function of phase space, P, i.e. space, angle, energy, and time. This section will briefly discuss current photon transport models and the numerical methods used to estimate the radiation flux distribution.

1.1.1 The Steady-state Photon Transport

We use the variable $\Psi(P)\ dP = \Psi(\vec{x}, \hat{\Omega}, E)\ d\vec{x}\ d\hat{\Omega}\ dE$ to represent the instantaneous track-length rate density of photons within dP about P. The radiation transport problem is often posed via the Boltzmann transport equation, which in steady-state simplifies to

$$\hat{\Omega} \cdot \vec{\nabla}\Psi(P) + \Sigma_t(P)\Psi(P) = \int \Sigma_s(P' \rightarrow P)\ \Psi(P')\ dP' + S(P) \qquad (1)$$

where Σ_t is the total interaction probability per unit distance traveled by a photon, $\Sigma_s(P' \rightarrow P)\ dP'\ dP$ is the probability per unit distance traveled of a photon within

dP' about P' scattering into an angle and energy within dP about P, and $S(P)\ dP$ is the rate of creation of photons within dP about P. Equation 1 represents a conservation of photons in the phase-volume dP about P: the first term denotes the net streaming of photons out of the spatial boundaries of dP; the second term refers to the removal of photons via interaction; the third term refers to the introduction of photons into P by scattering from other energies and angles; the fourth term generically describes the introduction of photons by fixed sources, such as radioactive materials or particle accelerators.

In some problems, we want to consider the "importance" of a photon at P to some response function, such as an expected detector response. The transport equation may be alternatively posed in terms of an adjoint equation, i.e.

$$-\hat{\Omega} \cdot \vec{\nabla}\Psi^*(P) + \Sigma_t(P)\Psi^*(P) = \int \Sigma_s(P \rightarrow P')\ \Psi^*(P')\ dP' + S^*(P) \qquad (2)$$

where $\Psi^*(P)$ represents the expected response of a photon at P and $S^*(P)$ denotes the response function of interest, such as the response cross section of a detector material or the fission cross section in a criticality problem. Note that, while physical photons are generated by radiation sources and down-scatter as they interact with matter, adjoint photons are created in the response region and up-scatter as they travel through material.

Painter et al. offer a third description of the transport equation, combining the ideas of forward flux and adjoint flux [Painter 1980]. The "contributon" flux is the number of photons within dP of P that eventually contribute to the detector, i.e.

$$\Psi^C(P) \equiv \Psi(P) \times \Psi^*(P) \qquad (3)$$

The contributon flux is therefore divergence-free in space except at the source and detector, since all contributon paths begin at the source and terminate at the

detector. Further details on the use of contributon modeling for shielding problems can be found in [Williams 1991], and [Seydaliev 2008] offers an example of modeling the contributon flux numerically.

1.1.2 Numerical Methods for Solving the Transport Equation

Numerical methods for solving the transport equation are generally categorized as deterministic or stochastic. Deterministic methods use finite-difference, finite-element, or finite-volume methodology to transform the integro-differential transport equation into a system of linear equations. While these approximations may achieve high-precision results faster than stochastic methods, they suffer from systemic discretization errors, such as ray effects, that are difficult to assess without expert judgment.

Stochastic or Monte Carlo methods solve the transport equation by statistically simulating a number of photons to obtain an estimate for the response of interest. Each photon is created by randomly sampling a birth location in the source domain and transporting it through the problem according to physical probability distributions. In this thesis, the word "history" is used to describe a Monte Carlo simulation photon.

Though Monte Carlo methods are intuitive and avoid errors like ray effects and convergence failure, they converge slowly when high precision is needed. In a Monte Carlo simulation, the histories' respective detector responses will have a statistical distribution with some standard deviation (σ). The central limit theorem indicates that as the number of sampled histories (N_{hist}) increases, the mean sample response ($\hat{X}$) will approach the true response with precision on the order of $\sigma/\sqrt{N_{hist}}$. Since the Monte Carlo simulation time (T) is expected to be proportional to N_{hist}, it is

convenient to establish a Figure of Merit for Monte Carlo simulations

$$FOM \equiv \frac{1}{R^2 T} \tag{4}$$

where R is the relative error in $\hat{X}$:

$$R \equiv \frac{\sigma}{\hat{X}} \tag{5}$$

Since R must be estimated with some statistical uncertainty, the FOM is also estimated with statistical uncertainty. The FOM estimate is expected to approach a constant value as N_{hist} approaches infinity.

Many widely-used Monte Carlo codes exist, including MCNP5 [MCNP 2008a], MORET4 [Nouri 1999], Geant4 [Geant4 2010], and MCBEND [Chucas 1994]. Using Monte Carlo methods to solve a simplified transport equation may improve efficiency when such approximations are appropriate. For example, introducing diffusion approximation to the transport operator can speed up Monte Carlo simulation when scattering is a dominant phenomenon [Densmore 2008]. Other codes couple deterministic and Monte Carlo solutions to take advantage of the deterministic simulation's speed and the Monte Carlo simulation's accuracy.

1.2 Monte Carlo Variance Reduction

Analog Monte Carlo refers to Monte Carlo simulation in which each history corresponds to a fixed number of physical photons. In many problems, the variance of responses relative to the true solution may be too high to make analog Monte Carlo a practical option [Smith 2005, Sheu 2008]. Several variance reduction methods exist to increase the statistical sampling of important regions (to reduce variance) while reducing the sampling in regions of low importance (to reduce runtime). The

MCNP manual divides variance reduction methods into truncation methods, partially deterministic methods, modified sampling methods, and population control methods [MCNP 2008a].

Simplifications (truncations) of the problem geometry or energy treatment can improve code efficiency. For example, terminating the simulation of histories below energies of interest or outside of the relevant spatial domain will reduce computation time while minimally distorting the solution. Other techniques may be used to take advantage of the symmetry of the problem, such as ring detectors [Booth 1985] or reflecting or periodic boundary conditions.

Partially deterministic methods circumvent the "random walk" Monte Carlo process in certain regions, using instead a deterministically calculated response. These methods include Deterministic Transport (DXTRAN), point tallies [MCNP 2008a], and other forced flight methods [Chucas 1994]. At every step of the random walk, these methods deterministically compute the probability of scatter from the local region to a region of interest and record the associated tally. Other approaches have coupled deterministic treatment of the transport through shielding regions with Monte Carlo treatment of detector response [Baker 1993, Smith 2008]. Another method, Variational Variance Reduction (VVR), could be included as a partially deterministic method. Codes employing VVR use a variational function to combine a forward solution and an adjoint solution (each of which may be found using deterministic or Monte Carlo methods) to obtain a higher-order estimate of the system response [Barrett 2001, Densmore 2002, Densmore 2004]. Becker describes a similar paired deterministic / Monte Carlo method in which Monte Carlo is used to correct errors in the deterministic solution [Becker 2007].

In modified sampling schemes, the random walk of each history is no longer

based on physical distributions alone. Therefore, modified sampling schemes must rely on the concept of history weight to maintain solution accuracy. One history can be used to represent more than one physical photon, (i.e., a history with twice the weight of another history represents twice as many physical photons). Modified sampling methods bias the sampling of transport phenomena, but compensate the weight of the transported history to maintain overall solution accuracy. For example, the exponential biasing method reduces the probability a history will scatter as it travels through a region of space, but decreases the weight of unscattered histories and increases the weight of scattered histories [MCNP 2008a, NEA 2008, Burn 1995]. Other methods implemented in MCNP include implicit capture, forced collisions [Booth 1985], and source biasing [Nouri 1999]. Several codes [NEA 2008, Burn 1995, Chucas 1994] have demonstrated biasing of the scattering kernel so that histories preferentially scatter toward high-importance regions.

Many of the modified sampling concepts have been combined in the Local Importance Function Transform (LIFT), which modifies the entire transport operator [Painter 1980, Williams 1991, Turner 1997a, Hoogenboom 2008]. Rather than model the forward transport equation, LIFT combines an *a priori* estimate of the adjoint flux with sampling distributions of the forward transport operator to model the contributon transport equation. If an exact adjoint solution were available, every Monte Carlo history would contribute the same amount to the detector response, resulting in a zero-variance solution. Some results for Monte Carlo LIFT modeling are available in [Turner 1997b].

Population control methods modify the sampling of phase space by terminating histories in unimportant regions and splitting histories in important regions. The weight of surviving histories is adjusted to maintain accuracy. Population control

can be applied in two ways: importance-based splitting or weight windows.

Importance-based splitting compares *a priori* importance estimates I_i and I_j of two regions i and j as a history travels out of i and into j. If I_j is larger than I_i, the history is split into roughly I_j/I_i independent sub-histories, each with weight reduced by a factor of I_i/I_j. If I_j is smaller than I_i, the history will play the roulette game: either be terminated (with probability $1 - I_j/I_i$) or survive with weight increased by a factor of I_i/I_j. Therefore, on average, the initial history weight w_i is conserved in the mean of all possible outcomes:

$$\langle w_j \rangle = \left(1 - \frac{I_j}{I_i}\right) \times 0 + w_i \times \frac{I_j}{I_i} \times \frac{I_i}{I_j} = w_i \tag{6}$$

Several examples are available from [Burn 1995], and MCNP uses importance biasing as a standard variance reduction method [Booth 1985].

The weight window method uses the same splitting and rouletting principles to conserve the weight of the initial history, but considers only the weight of the history compared to the weight window assigned to the region in which the history currently resides. This dictates, in theory, that all histories will reside in the local weight window as they travel through a region. In practice, weight windows are usually applied only at collisions, material interfaces, and occasionally along streaming paths to keep the associated cost reasonable. Section 2.4 further describes the practice of weight windowing.

1.3 Adjoint-Derived Weight Windows and Source Biasing

Several studies [Coveyou 1967, Wagner 1998, Haghighat 2003] argue that optimal weight windows are inversely proportional to the adjoint distribution. Intuitively, one may reason that more-important regions (i.e., those with higher adjoint)

should be sampled more frequently than those irrelevant to the problem. Recent research efforts have focused on weight windows generation schemes that seek to minimize the second moment of each history's contribution to the tally, explicitly seeking to minimize the variance of the solution [Booth 2010].

Several methods exist for automatically generating adjoint weight windows. A forward Monte Carlo run [Booth 1983, Booth 1984], perhaps with a modified source distribution [Shuttleworth 2000], can collect information about the fraction of photons in each region of phase space that contribute to the detector tally. Alternatively, a deterministic solution of the adjoint transport equation can be parsed into weight windows for use in a forward Monte Carlo run. This hybrid method has been implemented using deterministic diffusion [Mickael 1995, Gardner 1999, Garcia-Pereja 2007] and discrete ordinates [Van Riper 1997, Tang 1998, Wagner 1998, Wagner 2000, Shuttleworth 2000, Sweezy 2005, Peplow 2006, Sheu 2008] codes.

Regardless of the method of weight window generation, the use of a weight windows grid distinct from the problem geometry is preferred in most cases. Separating the problem into two discretizations allows adequate resolution of the weight windows distribution without encumbering the Monte Carlo engine with extraneous cell crossings [Liu 1997, Hendricks 2000].

1.3.1 The Consistent Adjoint-Driven Importance Scheme

In some problems, the importance function varies widely over the source domain [Wagner 1998, Hendricks 2000, Mosher 2010b]. When weight windows are applied to these problems, histories are frequently split or rouletted as they are born. This creates an implicit form of source biasing: in important regions the histories are

split at birth, creating a higher population of low-weight histories. In other regions the population is reduced.

This implicit source biasing is computationally expensive if many histories are terminated at birth; efficiency gains can be offered by explicitly biasing the source distribution such that every history is born in the local weight window. The consistent adjoint driven importance sampling (CADIS) method demonstrates that the source should be biased proportionally to the adjoint distribution [Wagner 1998].

To prevent the source biasing from affecting the tally mean, histories born in preferred regions are assigned reduced weight. For example, consider region i of the source in which some fraction p_i of the photons are generated. If region i is assigned a source biasing factor B_i, then a normalized fraction p_i' of the histories will be born in i, i.e.,

$$p_i' = \frac{p_i B_i}{\sum_j [p_j B_j]} \tag{7}$$

The fraction of photons born in region i must equal p_i; therefore, the weights of the p_i' histories born in region i are

$$w_i = \frac{\sum_j [p_j B_j]}{B_i} \tag{8}$$

Note that if rejection sampling is used, MCNP5 cannot properly estimate p_i. Therefore w_i will be inaccurate unless $B_i = 1$ for all regions, i.e., source biasing is not used [MCNP 2008b p. 3-59].

Several codes implement CADIS, including A^{3}MCNP [Wagner 2000], ADVANTG [Wagner 2002, Mosher 2010a], and MAVRIC [Peplow 2007] with good results. In these codes, volumetric sources are approximated by a series of biased point sources in MCNP, avoiding the conflict between rejection sampling and source biasing [Wagner 2000, Mosher 2010b].

1.3.2 Forward Weighted CADIS

In problems where multiple regions of interest exist, the adjoint source must be balanced so that the flux in each region of interest is sampled adequately. The forward weighted CADIS (FW-CADIS) method accounts for the forward flux distribution when calculating the strength of each adjoint source [Wagner 2007, Peplow 2007, Mosher 2009, Mosher 2010a]. Wagner notes that the FW-CADIS's requirement of forward and adjoint deterministic solutions is very economic compared to the cost of running a separate Monte Carlo calculation for each detector [Wagner 2009].

1.4 Source/Detector Approaches

Transport problems are frequently categorized by the scope of their region of interest. For example, global problems require flux estimates over a large region of the problem; the eigenvalue of interest in criticality problems is strongly affected by the flux in highly multiplicative regions of the core. This thesis focuses on source/detector problems, in which a small region of interest is defined within a larger physical model. Many problems fit this description, including nuclear oil-well logging, passive assay, and radiography models. Source/detector problems may be further categorized based on how widely the importance function varies over the source domain; thickness of shielding between the source and detector; and the relative contribution of streaming paths to the overall result.

The importance of a region depends on the presence of paths from that region to the region of interest. In some problems of interest, such as ex-core detector or cask shielding applications, the importance function varies substantially over the source

domain [Wagner 1998, Haghighat 2003, Mosher 2010b]. In these cases, CADIS methodology is important to ensure efficient sampling of the source distribution.

While the Monte Carlo efficiency is generally insensitive to the adjoint solution quality [Haghighat 2003], some important exceptions exist. Gardner found that better efficiency was achieved by generating weight windows from deterministic solutions than forward Monte Carlo runs [Gardner 1999]. The benefit is lost for problems with highly angle-dependent importance functions [Sweezy 2005], unless angle-dependent weight windows are also applied [Booth 1983, Van Riper 1997, Peplow 2010]. In some cases, steps must be taken to generate sufficiently accurate weight windows in streaming regions [Shuttleworth 2000].

Overall, the degree to which adjoint weight windowing improves the FOM for source/detector problems depends on problem attenuation, presence of streaming paths, use of source biasing, and choice of weight window generation method. An ideal variance reduction scheme could provide an accurate and efficient solution with no user interaction or expert judgment needed. Several studies note that expert judgment is often called for, especially in considering the possibility of false convergence (in which the precision of the solution is over-estimated because important paths have been under-sampled) [Booth 1985, Hendricks 2000]. Efforts have been made to simplify the decision-making process, including statistical checks in MCNP5 [MCNP 2008a] and automatic weight windows generation.

1.5 Thesis Overview

In several source/detector problems of interest to the nuclear nonproliferation community, the adjoint weight windowing method insufficiently improves the FOM. This thesis aims to identify the causes for weight windowing's diminished

performance in these problems so that solutions can be devised and perhaps incorporated into an automated variance reduction package. The remainder of this thesis is organized as follows:

II. The hybrid method used in this thesis is described in Chapter 2. First, the adjoint flux is deterministically solved using Transpire's Attila^{TM} code [Wareing 2001]. Next, Attila^{TM} generates adjoint weight windows for MCNP5. The user must create source biasing parameters using an empirical method. Finally, the Monte Carlo simulation is performed.

III. In Chapter 3, two source/detector case studies, including one with a relatively small source domain and one with a relatively large source domain, are considered. Test Case I is used for two trials in which the FOM is recorded as a function of the adjoint solution quality and shielding density, respectively. Test Case II quantifies the improvement in FOM when appropriate source biasing is used for a problem of interest to the nonproliferation community. Results from the method developed in Chapter 2 are presented.

IV. In Chapter 4, conclusions of the case studies are presented. The results in Chapter 3 suggest that weight windows should monotonically decrease along relevant paths from the source to the detector. The appropriate use of source biasing, such as the CADIS method, is critical for problems where the importance varies greatly in the source domain. Finally, a comparison of weight windowing with LIFT explains how LIFT's scatter-angle biasing may be important when large streaming regions exist near the detector.

V. In Chapter 5, several directions for future research are described. For problems where precise results are desired in many energy groups, the FW-CADIS

method could be applied to energy instead of position. A method is described for generating weight windows that more appropriately use the adjoint solution information. Finally, a new "F0" tally for allowing source biasing with rejection sampling is described.

2 Methods

2.1 Introduction

Although the idea of adjoint-derived weight windowing is well-established, there is need to determine the limits of the method and reasons for the decline in its effectiveness. The methods outlined in this chapter are intended to allow adjoint-derived weight windowing in the best way possible while shedding light on the problems that limit the domain of problems over which weight windowing improves the FOM.

First, Attila^{TM} is used to simulate the adjoint flux and generate weight windows. Special care is taken to prevent nonphysical adjoint flux solutions in regions relevant to the solution. Source biasing is applied to preferentially sample regions where the weight windows are low. Since MCNP5 does not derive source biasing directly from weight windows and Attila^{TM} does not generate source biasing parameters, the source biasing parameters are generated empirically by the user. Finally, MCNP5 simulates the flux in the detector.

2.2 Deterministic Adjoint Solution

Transpire's Attila^{TM} version 7.0.0 code is used to deterministically solve the adjoint solution and generate weight windows. Cross sections used in Attila^{TM} were generated using the CEPXS libraries installed in RADSAT [Smith 2008]. Although some coded features of Attila^{TM} are proprietary, the tools of interest will be described in this section.

Attila™ uses tetrahedral meshing to discretize the spatial domain of the problem, discrete ordinates treatment of angular dependence, and multigroup treatment of the energy variable [Attila 2009]. The spatial distribution is represented using discontinuous finite element spatial differencing. The scattering source is stored as an expansion of spherical harmonic moments, which is updated between "sweeps" of the spatial mesh.

The deterministic adjoint solution is considered converged when all regions with importance above 10^{-4} times the importance of the source location are well-resolved. If the solution appears rough or nonphysical, a finer mesh or angular treatment may be required.

2.3 Creating Weight Windows

Attila™ can automatically generate a weight window map for MCNP. The user specifies the number of mesh divisions in each of the three Cartesian directions, and a normalization constant C_{ww} for the weight windows. The number of divisions is chosen so that each division is approximately one mean-free-path for the photon energy group with the longest mean-free-path. The normalization constant C_{ww} is chosen to prevent information in the deterministic adjoint solution with high relative error from affecting the Monte Carlo run, as described in this section.

Attila™ uses C_{ww}, the number of divisions, and the deterministic solution to generate weight windows. For each hexahedral cell in the weight window file, Attila™ uses the following method to find an appropriate weight window: first, Attila™ finds the solution at each of the eight vertices of the hexahedral cell by evaluating the finite element solution at those points. The mean of these

eight adjoint fluxes estimates the average adjoint flux in the hexahedral cell, Φ^*. Attila^{TM} then assigns a weight window lower bound inversely proportional to the adjoint flux, up to 10^{10}, i.e.,

$$ww_l = min\left(\frac{C_{ww}}{\Phi^*}, 10^{10}\right) \tag{9}$$

These values are stored in a text file that MCNP can read.

Very often if the adjoint flux is very close to zero, the relative error of the deterministic solution will be significant. (Negative adjoint flux values may exist, which is an unphysical phenomenon.) The upper bound in Eq. 9 provides a convenient way to ignore portions of the deterministic solution that are below a certain threshold. To disable weight windowing in these regions (which, if the deterministic solution has been properly resolved as per Section 2.2, will have little impact on the tally of interest), the user sets C_{ww} so that ww_l in the regions to be disabled falls above the 10^{10} threshold. For example, the user could set $C_{ww} = 10$ to force constant weight windows for adjoint solution values below 10^{-9} in Fig. 1.

2.4 Source Biasing

By default MCNP5 applies weight windows at birth. "Perfect" weight windows would be an exact inversion of the adjoint flux, and the weight windows would be "narrow" if the window had no width, i.e., all histories at P would be split or rouletted to one weight. If perfect, narrow weight windows were applied at birth, the result would be an "implicit" biasing of source histories (following the first weight windows application) proportional to the adjoint flux. Each surviving history would have its weight modified so that the weight of all histories born in a region of phase space is equal to the weight born in the same region in

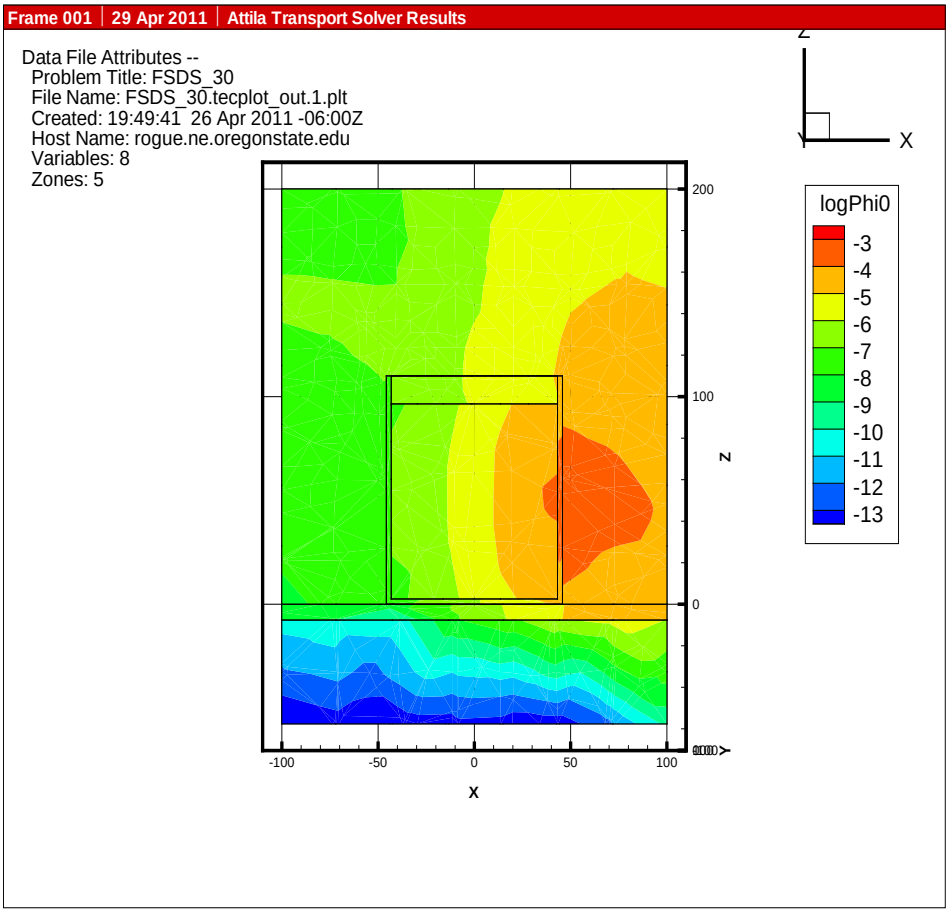

Figure 1: A slice of an example adjoint solution with ray effects perturbing the solution below 10^{-9} (light blue).

an analog simulation. As described in this section, however, perfect and narrow weight windows cannot and should not be used. Explicitly defining source biasing parameters (rather than relying on weight windows to implicitly bias the source) therefore offers an improvement in the Monte Carlo FOM in problems where the importance function varies widely over the source domain.

MCNP5 weight windows are isotropic and fail to capture the angular dependence of the adjoint flux distribution. Similarly, the simplification of the spatial dependence from a fine tetrahedral mesh to a coarser hexahedral mesh reduces the resolution of the adjoint solution. The advantages of these simplifications are that they greatly reduce the memory requirements for storing the weight windows and reduce the cost associated with applying the weight windows.

Using isotropic weight windows limits the effectiveness of angular source biasing. If histories are preferentially born in certain directions with smaller weight, rouletting will be applied to these histories (or other histories will be split) so that the source biasing is negated.

Also, the weight windows are not narrow. MCNP5 defaults to set the upper limit of the window at 5 times the lower limit. Using wide windows is important because it prevents excessive rouletting and splitting of histories due to small changes in the importance function. Page 2-148 of [MCNP5 2008a] indicates that, based on empirical evidence, the default window width "works well, but the FOM is reasonably insensitive to this choice...." Therefore the default window width is used throughout this thesis.

Using wide windows means that histories can exist anywhere within that window, meaning a range of weights may be found in one region of the problem. This offers the user flexibility in applying angular source biasing: important directions

may be sampled up to 5 times more often than unimportant directions.

By default, splitting and rouletting are applied in no more than a 5:1 ratio. In other words, a history is split no more than five-fold, and survives a roulette game at least 20% of the time. This limitation is intended to prevent nonsensical splitting. For example, a history may take a path around a shield and scatter into a region with very high importance. In this case, excessively splitting this history is unlikely to reduce its contribution to the problem variance but will incur significant computational cost and therefore reduce the FOM. (Booth gives another example in slide 42 of [Booth 2010].) Additionally, excessive rouletting — perhaps a result of underestimating the importance of a path from the source to the detector — can allow relevant paths to be inadequately sampled, resulting in a false appearance of solution convergence.

Limiting the application of weight windows can severely interfere with implicit source biasing. Consider histories born far below the local weight window: Although many are terminated at birth by the roulette game, 20% will survive with 5-fold increased weight. These will be transported through the problem until weight windowing is applied again, presumably still in a low-importance region of the problem. Eighty percent of these histories will be terminated here. (The remaining 20% — 4% of the histories born in the low-importance region — will be transported further.) The result is that computational effort is wasted transporting histories that are unlikely to contribute information to the solution.

The source biasing methods used in this thesis attempt to take advantage of MCNP5 features to maximize the FOM by matching the source biasing distribution to the adjoint flux distribution.

2.4.1 Case I: Point Source

When the importance function is fairly constant across the spatial domain of the source, the birth weight of histories should fall within the local weight window. If the weight windowing parameters are known at the source location, it is simple to use energy biasing and the WGT parameter of the SDEF card to match the source weight distribution to the weight windows exactly.

When angular source biasing is used, the histories' birth weights are decreased in preferred directions and increased in non-preferred directions. It is likely that not all birth weights can fall within the weight window. In this case, a binary search is used to find the ideal compromise between splitting and rouletting at birth.

MCNP5 prints a warning indicating how many histories are born above and below the local weight window. This warning allows the user to quickly bound the domain of the ideal WGT parameter. To find the upper bound, the user simulates 1000 histories with an initial guess for WGT. If roughly 99% of the histories are born above their weight window, that value of WGT is a good upper bound for the optimization search. Otherwise WGT is changed and the simulation is performed again. A similar method is used to find the lower bound for the optimization search.

To perform the binary search, the FOM is noted at the upper and lower boundaries of WGT and at three logarithmically equidistant values between the upper and lower boundaries using the preliminary simulation procedures described in Section 2.5. The FOM measurements are not expected to smoothly vary with WGT (since they are subject to statistical variance) but should give a clear indication which of the five WGT values offers the highest FOM. The neighboring values of

WGT become the new boundaries of the binary search. For example, if a series of five FOM values were simulated as depicted in Fig. 2, the user would reason that the ideal WGT would exist between 10 and 10^3. The five values next considered

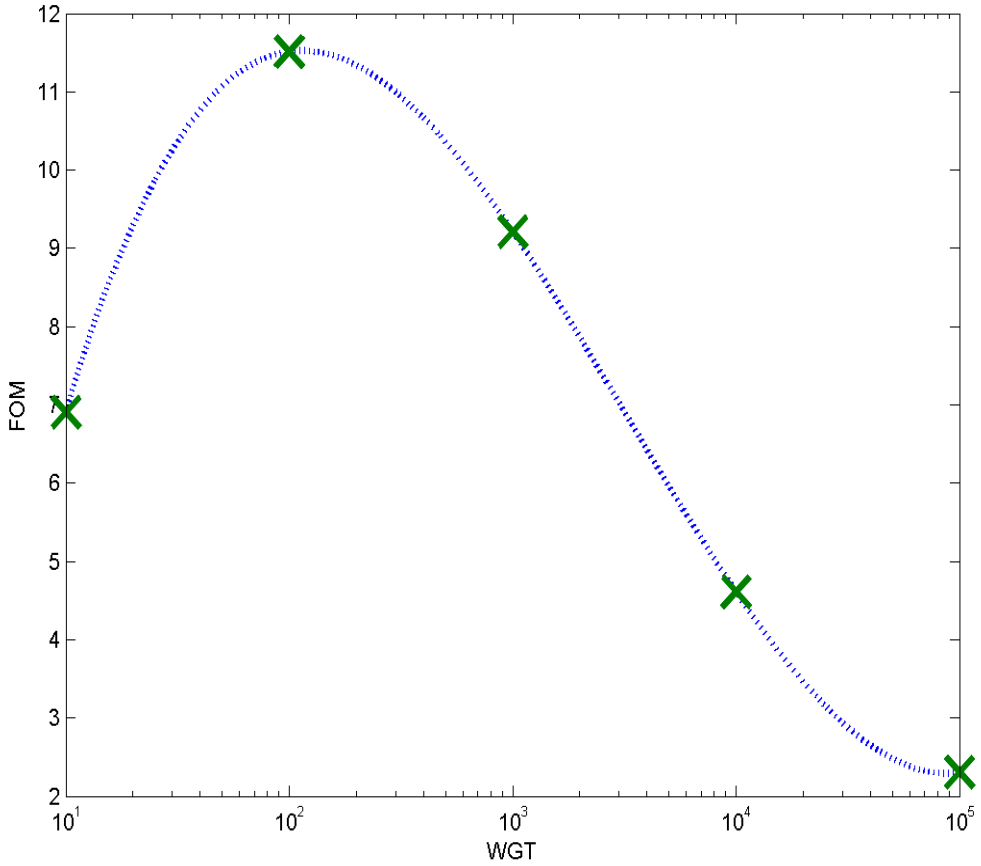

Figure 2: An example of data recorded in the search process used to find the ideal WGT parameter.

would be 10, $10^{1.5}$, 10^2, $10^{2.5}$, and 10^3. The search is terminated when the optimal WGT is bounded within an order of magnitude or the differences in FOM among the five points is no longer statistically significant.

2.4.2 Case II: Volumetric Source

When the importance function varies significantly over the source domain, steps must be taken to match the source biasing distribution to the weight windows distribution. Ideally the biasing distribution would be proportional to the deterministic importance function, so that every history would be born in the local weight window. This is not possible, because MCNP5 only allows the biasing function to depend on the three Cartesian coordinates independently. (The A^{3}MCNP [Wagner 2000] and ADVANTG [Mosher 2010b] codes implement source position biasing by representing the source volume as a series of points with independent biasing parameters.) In this thesis, the source biasing is matched to the importance function using empirical corrections to a logical initial guess.

Neglecting scatter, the importance function decays exponentially through shielding material. A reasonable guess for the source position biasing distribution is therefore an exponential distribution with decay rate based on measurements of the adjoint flux from the deterministic adjoint solution. MCNP5 allows source biasing in each of the Cartesian directions independently. For this thesis, the initial guess for the biasing distribution will be exponential in the direction from the detector to the source, and constant with respect to the other two directions. This initial guess is used to find the ideal WGT, as described in Section 2.4.1.

Once the ideal WGT is established, similar binary searches are used to find the ideal decay rate for the exponential biasing distributions. It is assumed that the optimal decay parameter in one direction is not affected by the parameter used in the other direction; this assumption was demonstrated as reasonable by re-performing the binary search using the optimal parameters and arriving at the same parameters.

2.5 Monte Carlo

The Monte Carlo portion of the hybrid method used Los Alamos National Laboratory's MCNP5 version 1.51 on the Windows 7 operating system. Since the MCNP5 FOM is one of the important metrics of success, care was taken to provide consistent processing power and memory for each simulation. A Dell™ Precision™ M4400 with 4.00 GB of random access memory (RAM) and a 2.53 GHz Intel® Q9300 four-core central processing unit (CPU) was used to perform the MCNP5 simulations. No more than three simulations were performed simultaneously, and each simulation used only one core. Therefore each MCNP5 simulation had exclusive use of one core, while the computer operating system and auxiliary programs were handled by the fourth core. The available RAM exceeded simulation requirements in all cases.

2.5.1 Monte Carlo Stopping Criteria

Since this thesis is interested in the mean of each tally as well as the FOM (which is derived from the relative error), the Monte Carlo solution must assess both with sufficient precision. The number of histories used in the simulation must be sufficient so that R and the relative error *of the relative error* (ROR) are sufficiently small. One can apply the propagation-of-uncertainty relationship to Eqn. 4 to estimate the standard error of the FOM estimate:

$$\sigma_{FOM}^2 = \sigma_R^2 \left(\frac{\partial\ FOM}{\partial R} \right)^2 = \sigma_R^2 \left(\frac{-2}{TR^3} \right)^2 = 4\ FOM^2 \left(\frac{\sigma_R}{R} \right)^2 \tag{10}$$

where σ_{FOM} is the standard error of the FOM estimate and σ_R is the standard error of R. Since $ROR \equiv \sigma_R/R$ and MCNP5 reports the variance of the variance ($VOV \equiv ROR^2$) [MCNP 2008a p. 2-122] instead of ROR, we can rewrite Eq. 10

to show that the relative error in our estimate of the FOM is

$$\frac{\sigma_{FOM}}{FOM} = 2\sqrt{VOV} \tag{11}$$

When searching for optimal WGT or source biasing parameters in preliminary simulations, relative error in the FOM estimate of less than 20% was considered sufficiently precise; therefore the simulation must aim to achieve $VOV < 0.01$. After the ideal simulation parameters are chosen, one conclusive simulation was run, targeting R less than 5% and relative error in the FOM of less than 10%; therefore the simulation must achieve $R < 0.05$ and $VOV < 0.0025$.

Monte Carlo simulations ended after one of several stopping criteria was met: All simulations were initially run for 5 minutes of CPU time using the CTME card. If the solution did not meet the conditions in the previous paragraph, the simulation was continued for an additional time that was expected to exceed the precision requirements (based on the $1/\sqrt{N_{hist}}$ convergence of R and the $1/N_{hist}$ convergence of VOV). No more than 60 or 600 minutes of CPU time were allowed for preliminary and conclusive simulations, respectively.

2.5.2 Post-Processing

As described in Section 2.4, WGT was chosen to match the weight windows. Adjusting the mean history birth weight will proportionally increase the tallies in the simulation. To make the results comparable with one another, each tally was divided by the WGT parameter in post-processing.

3 Results

3.1 Introduction

The methods described in Chapter 2 were applied to two problems of interest to the nuclear safeguards community. The problems were constructed by collaborators at Pacific Northwest National Laboratory. The first problem is a collimated barium-133 point source, shielded by low-Z material of varying densities. The second problem is the passive assay of a pressurized uranium hexafluoride (UF_6) cylinder using a photon detector. Problem descriptions and results from these simulations are given in this chapter.

3.2 Test Case I Description: Mulch Crate

Active interrogation is currently used for screening small luggage, and its role is expanding to include larger cargo items [Miller 2010]. Although these active interrogation scenarios vary in optical thickness and exact geometry, many are conceptually similar from a radiation transport perspective. Therefore, although the mulch crate problem has limited direct use for the safeguards community, it is representative of many radiography problems.

The layout of the mulch crate problem is shown in Fig. 3. In this problem, the Attila^{TM} mesh size is varied to change the quality of the adjoint solution. In another set of trials, the mulch material density is varied from 0.266 g/cc up to 2 g/cc to consider a variety of shielding thicknesses encountered in other problems. A barium-133 photon spectrum was used. (Photons in low-Z material frequently

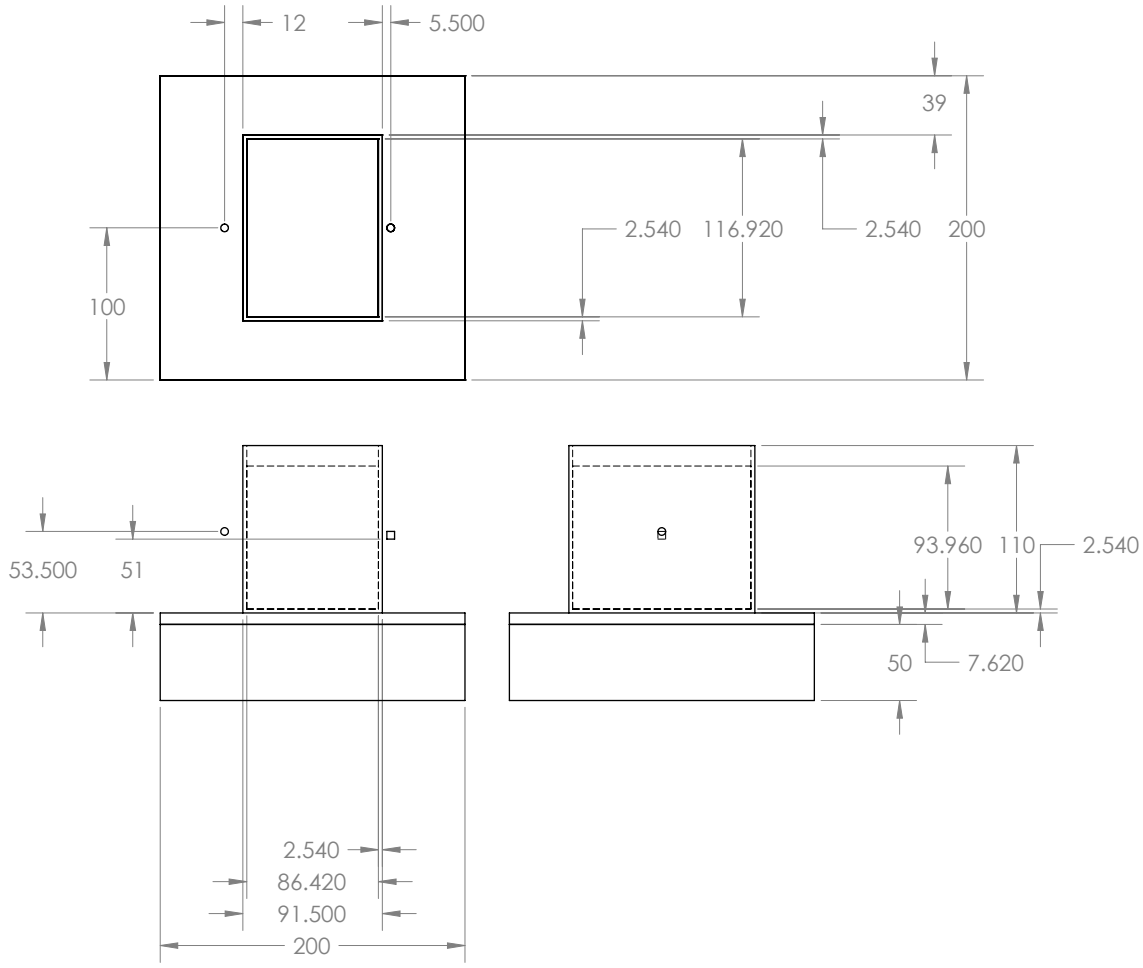

Figure 3: The top, front, and side views of the mulch crate model show Test Case I consists of a point source (sphere at left), shielding region, and detector region (cylinder at right).

undergo Compton scatter.)

3.2.1 Test Case I Specifications: Attila™

The Attila™ model is simplified to model the essential features of the problem without burdening the simulation with features that have little impact on the Monte Carlo simulation. Since the detector is very small, it will be treated as a point source for the adjoint flux. Attila™ uses a ray-tracing algorithm to simulate the uncollided adjoint flux from the point source. A "first-scatter distributed source" (FSDS) is generated from the ray trace to serve as a source for the deterministic calculation. The settings used for the deterministic calculation and associated adjoint calculation are recorded in Tables 5 through 7 of Appendix A.

The adjoint flux moments generated by the deterministic calculation are used in a report-only calculation to generate weight windows. Table 8 of Appendix A notes the modifications made to the deterministic calculation to generate weight windows.

3.2.2 Test Case I Specifications: MCNP5

The MCNP5 model adds a small detector region to the Attila™ model. The geometry portion of the mulch MCNP5 input is included as Table 9, and the material compositions used are included in Table 10. (See Appendix A.)

The photon source is located at $\vec{x} =< -57.75, 0, 53.5 >$. The source direction distribution is linearly anisotropic (toward the $\pm\hat{i}$ directions, where $\hat{i}$ is the unit vector along the x-axis) with quadratic source biasing toward $\pm\hat{i}$. In other words,

histories were distributed with probability density

$$P(\mu) = \frac{|\mu^3|}{2} \tag{12}$$

where μ is the dot product of $\hat{\Omega}$ with $\hat{i}$, and the weight of each history was corrected by a factor of

$$w(\mu) = \frac{2}{\mu^2} \tag{13}$$

to make the distribution linearly anisotropic. The WGT parameter is set differently for each case to match the weight window at the source position, as described in Section 2.4.1. The source energy distribution is entered as a histogram and is described in Table 11 of Appendix A. Although the true distribution would be a discrete series of values, the inconsistency is not expected to affect the results of this study; the Monte Carlo results and FOM will be similar to those using the barium-133 spectrum because the simulated radiation is in the same regime and will experience similar scattering and absorption.

An F4 tally was applied to tally photon flux in cell 500. Energy-dependent tally information was not used in this study. Only photons are transported, with importances of unity in all cells except for the "universe" cell that demarcates the vacuum boundary of the problem. The weight-windowing parameter card is used to direct MCNP5 to look for an external weight-window file.

3.3 Test Case I Results

Test Case I is used in two sets of simulations to determine the characteristics of the adjoint solution that could reduce the FOM when using weight windowing. In the first set of simulations, the quality of the adjoint solution is controlled by the

spatial mesh size. In the second set of simulations, the shielding density is varied. Increasing the shielding thickness reduces the fraction of photons that reach the detector and increases the relative importance of photon paths that scatter around the crate and reach the detector.

3.3.1 Effect of Adjoint Solution Quality on FOM

In the first set of Case I simulations, the spatial mesh size in the deterministic calculations is varied from 5 to 60 cm to understand the effect of deteriorating adjoint solution quality on the FOM. The mulch density was 2.0 g/cm^3 in every simulation. Results from the mulch crate simulations of varying deterministic mesh sizes are summarized in Table 1, including a trial with no weight windowing ("analog") and the ratio of the largest single-history contribution to the mean non-zero contribution ("Contribution Ratio"). Although the FOM is an unreliable indicator here due to high-weight contributions, note the significant decrease in the number of histories reaching the detector between Trials 3 and 4. The number of histories reaching the detector per minute of CPU time has a strong effect on the FOM as N_{hist} approaches infinity. (All trials in Table 1 used 600 minutes of CPU time.) Figures 4 and 5 depict the two numerical solutions, offering insight into the cause of decrease in the number of contributing histories.

3.3.2 Effect of Shielding Density on FOM

In the second set of Case I simulations, the shielding density is varied from 0.266 to 2.0 g/cm^3 to investigate the effect of increased shielding on the FOM. The mesh size was 30 cm by default, but was decreased as needed to avoid numerical inaccuracy such as the nonphysical solution depicted in Fig. 5. Results from the

Test Case I Results at Varying Mesh Sizes						
	Analog	Trial 1	Trial 2	Trial 3	Trial 4	Trial 5
Mesh Size (cm)	n/a	5	10	15	30	60
Adjoint Mesh Cells	n/a	638724	85746	29075	10963	1321
MCNP5 Histories (N_{hist})	532233837	79125927	100640202	79195341	78414366	76396178
Tally	0	1.0724E-10 ±21.00%	6.2907E-10 ±77.2%	7.9810E-11 ±11.83%	1.1964E-10 ±41.91%	1.3883E-10 ±38.08%
FOM	n/a	0.032 ±159.9%	0.0028 ±199.1%	0.12 ±87.5%	0.0095 ±195.5%	0.011 ±185.4%
Contributing Histories	0	1724	2060	1322	816	320
Contribution Ratio	n/a	3.2302E+02	1.5870E+03	9.7363E+01	3.3809E+02	1.1728E+02

Table 1: Results from MCNP5 runs of the mulch problem at various mesh sizes after 600 minutes of simulation time

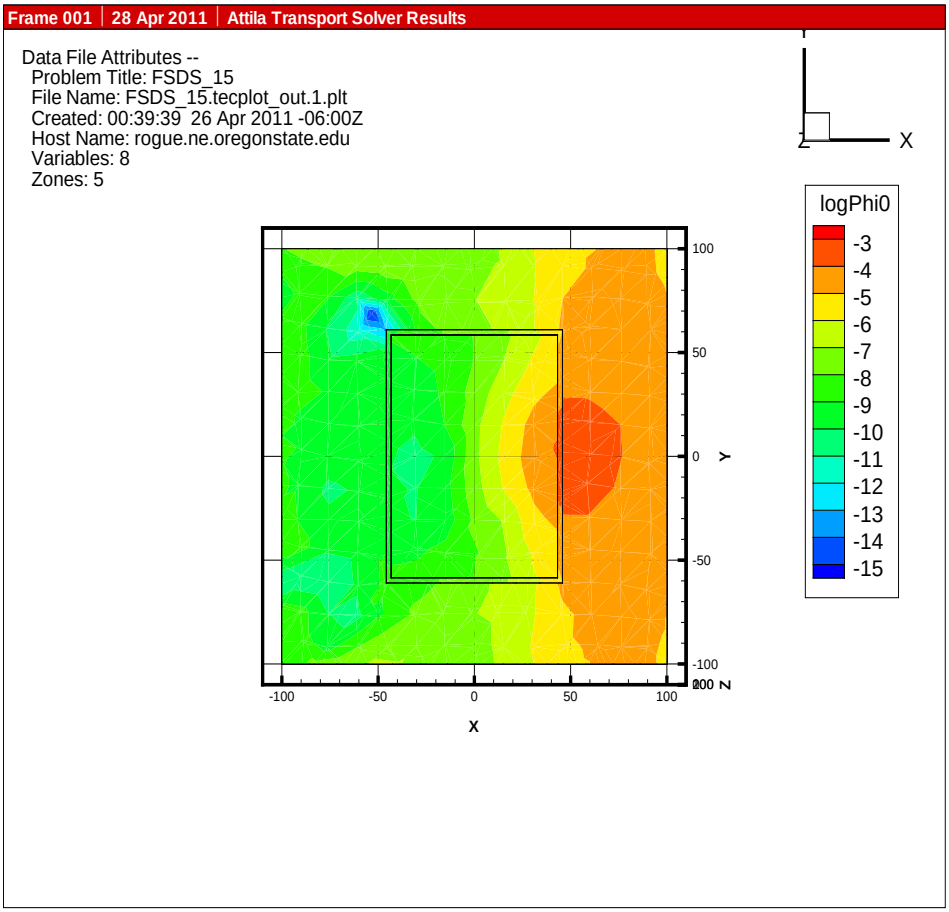

Figure 4: A false-color plot of the deterministic adjoint flux solution at $z = 71.19$ cm above the concrete slab with a mesh size of 15 cm. Compare to Fig. 5.

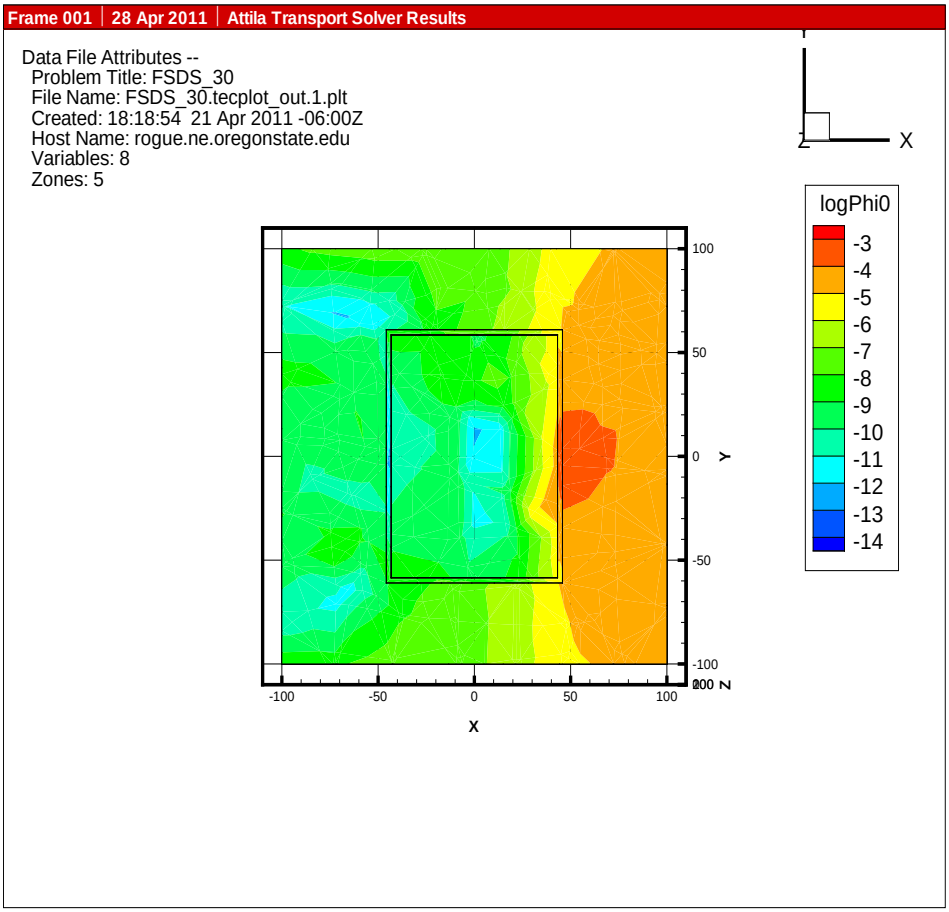

Figure 5: A false-color plot of the deterministic adjoint flux solution at $z = 71.19$ cm above the concrete slab with a mesh size of 30 cm. Compare to Fig. 4.

Test Case I Results at Varying Mulch Densities				
	Trial 0	Trial 1	Trial 2	Trial 3
Shielding Density (g/cm^3)	0.266	0.5	1.0	2.0
Shielding thickness (mean free paths)	2.33	4.37	8.74	17.49
Deterministic Mesh Size (cm)	30	30	30	15
MCNP5 Histories (N_{hist})	10^7	10^7	10^8	323277310
Tally	6.2833E-06 ±3.09%	2.0825E-06 ±3.26%	9.0865E-08 ±1.81%	1.6229E-10 ±18.02%
FOM	271 ±18.4%	296 ±33.5%	136 ±70.1%	0.051 ±166.3%
Results Without Weight Windowing (Analog)				
MCNP5 Histories (N_{hist})	4×10^7	4×10^7	4×10^7	532233837
Tally	6.6743E-06 ±3.33%	2.0484E-06 ±6.04%	1.0353E-07 ±24.62%	0
FOM	66 ±8.9%	19 ±14.4%	1.1 ±54.9%	0

Table 2: Results from MCNP5 runs of the mulch problem at various mulch densities

mulch crate simulations of varying mulch densities are summarized in Table 2.

In Table 2, note the significant decrease in FOM between Trials 1 and 3. Figures 6 and 7 depict the two adjoint solutions, offering insight into the cause of decrease in Monte Carlo FOM.

In several instances during the MCNP5 runs, the FOM suddenly decreased because a single high-weight history contributes an amount on the order of 10^4 larger than the average contribution, e.g., Fig. 8. "Table 160" in the MCNP5 results identifies the history with the largest contribution to the tally, and the DBCN card allows the user to print a detailed log of that specific history. Logs for the high-contribution histories showed that they often scattered in or near the

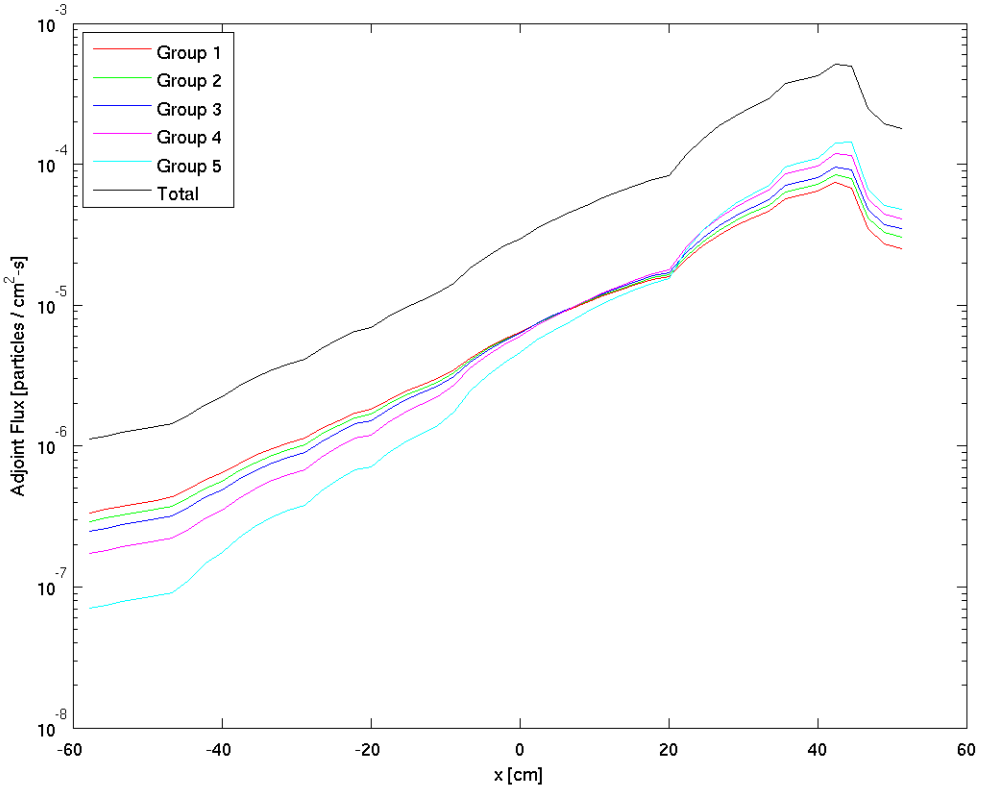

Figure 6: A plot of the energy-dependent scalar adjoint flux solution along a line from the source ($\vec{x} =< -57.75, 0, 53.5 >$) to the detector ($\vec{x} =< 51.25, 0, 51 >$) with shielding density 0.5 g/cm^3. Compare to Fig. 7.

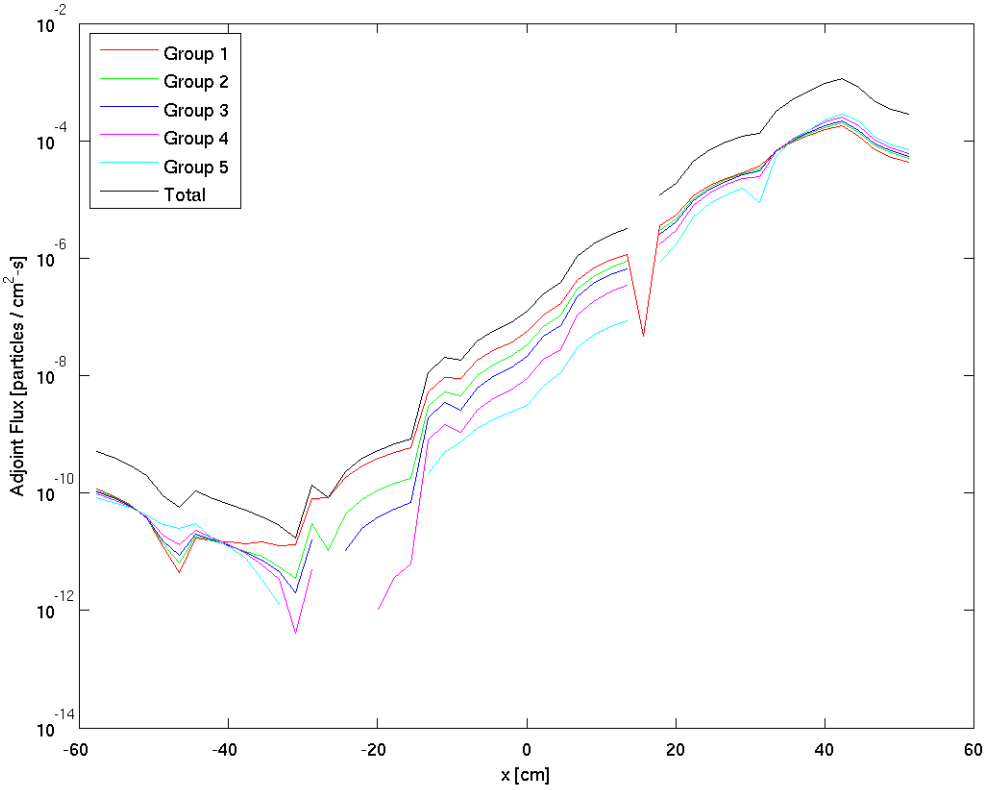

Figure 7: A plot of the energy-dependent scalar adjoint flux solution along a line from the source ($\vec{x} =< -57.75, 0, 53.5 >$) to the detector ($\vec{x} =< 51.25, 0, 51 >$) with shielding density 2.0 g/cm^3. Compare to Fig. 6.

tally 4

nps	mean	error	vov	slope	fom
8192000	8.7178E-02	0.0420	0.0096	10.0	312
16384000	8.8502E-02	0.0410	0.2676	4.1	163
24576000	8.7594E-02	0.0316	0.1591	4.2	183
32768000	8.7924E-02	0.0267	0.1004	3.3	192
40960000	8.7905E-02	0.0231	0.0736	3.1	204
49152000	8.8616E-02	0.0210	0.0533	2.9	205
57344000	9.1757E-02	0.0275	0.2054	2.5	103
65536000	9.1253E-02	0.0248	0.1845	2.3	111
73728000	9.1327E-02	0.0228	0.1634	2.4	117
81920000	9.1518E-02	0.0210	0.1465	2.5	124
90112000	9.1559E-02	0.0196	0.1323	2.5	129
98304000	9.1134E-02	0.0184	0.1238	2.8	135
100000000	9.0865E-02	0.0181	0.1228	2.8	136

Figure 8: A screenshot showing a large single-tally contribution to the detector between histories 49152000 and 57344000.

concrete slab, often within a few mean free paths of the detector.

3.4 Test Case II Description: Uranium Hexafluoride Cylinder

The second test case considered in this thesis is the passive interrogation of a UF_6 transport cylinder. Rapid non-destructive assay of isotopic composition is an important tool in the accounting of nuclear material for safeguards purposes. Measurements similar to the one simulated may be used to determine isotopic composition of the uranium material within the cylinder, which would provide inspectors with information to consider the overall intent of a foreign nuclear program. This Monte Carlo simulation is challenging because the dense high-Z UF_6 material very effectively shields photons, especially the low-energy photons characteristic of uranium-235. The UF_6 problem is sketched in Fig. 9 and dimensioned in Figs. 12

through 14 of Appendix B. Results were generated using the F4 track-length tally, although an F8 pulse height tally is more useful for radiography simulation.

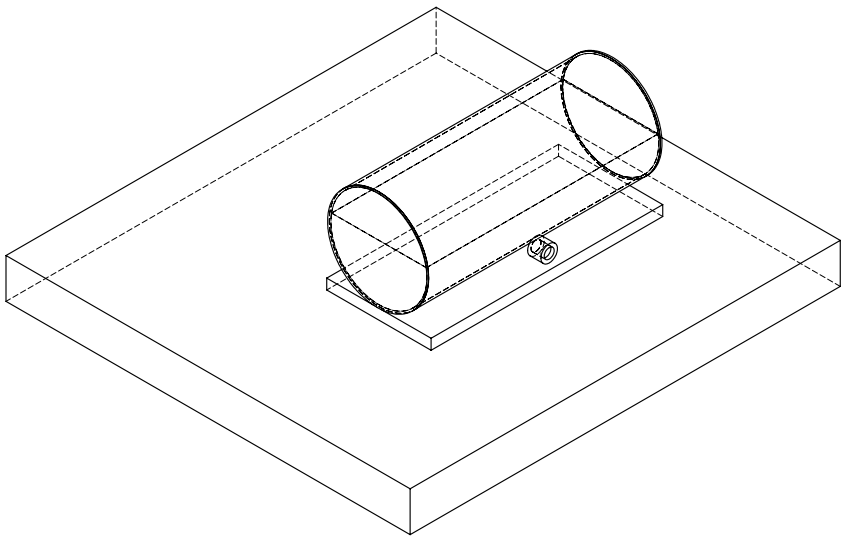

Figure 9: An isometric view of Test Case II shows the partly-filled UF_6 cylinder suspended above a "cart" and a large concrete slab. The small detector cylinder has a recess in its right side.

3.4.1 Test Case II Specifications: Attila™

As in Test Case I, a first-scatter distributed source (FSDS) calculation is used to approximate the detector region as a point detector. (The detector is the adjoint source.) The settings used for the FSDS calculation and associated adjoint

calculation are recorded in Tables 12 and 13 of Appendix B.

The flux moments generated by the FSDS calculation are used in a report-only calculation to generate weight windows. Table 14 of Appendix B notes the modifications made to the FSDS calculation to make the weight-window-generating calculation.

3.4.2 Test Case II MCNP5 Input

The MCNP5 model for Test Case II adds considerable detail to the Attila™ model. The geometry portion of the UF_6 MCNP5 input is included as Tables 15 through 18 in Appendix B. MCNP5 uses translation cards to easily reposition surfaces. The cart (TR 111) was not translated. The detector apparatus (TR 211) was translated by $< 0, 43, 60 >$ and rotated 90° about the positive x-axis. The material compositions used are included in Table 19 of Appendix B.

The photon source is defined on the domain

$$\left\{ \vec{x} =< x, y, z > \left| -88.9 \leq x \leq 88.9 \bigcap -36.83 \leq y \leq 36.83 \bigcap 34.29 \leq z \leq 76.97 \right. \right\} \tag{14}$$

Any histories born outside of cell 8521 are rejected and sampled again. The uranium-235 gamma spectrum used to define the source is given in Tables 20 and 21 of Appendix B.

An F4 tally was applied to estimate photon flux in Detector 3 (cell 230). Only photons are transported, with importances of unity in all cells except the "universe" cell. The weight-windowing parameter card directs MCNP5 to look for an external weight-window file.

Optimal source biasing parameters were found using a binary optimization

search on each of the independent parameters. Since an exponential decay of importance is assumed, the biasing parameters take the form

$$B_i = \frac{B_{i-1}}{C_{SB}} \tag{15}$$

where grid cell $i-1$ is nearer to the detector than adjacent grid cell i, C_{SB} approximately accounts for angular and attenuation effects in the x, y, or z direction. The values are normalized so that

$$\sum_i B_i = 1 \tag{16}$$

for x, y, and z separately.

3.5 Test Case II Results

The grid and optimal C_{SB} values are listed in Table 3 and plotted in Fig. 10. Results from the UF_6 runs are summarized in Table 4. Because of the problem's

Test Case II Source Biasing Distribution		
Direction	***Number of Grids***	***Optimal*** C_{SB}
x	18	2.5
y	8	3.5
z	8	1.0

Table 3: Details on the biasing parameters for Test Case II as a function of x, y, and z

unique geometry, biasing as a function of height did not produce any statistically significant benefit in preliminary simulations. Therefore results from Trials 3 and 4 are identical.

Note that the tally does not converge on the correct mean when source biasing is used. This is expected, since MCNP5 is not capable of using source biasing with

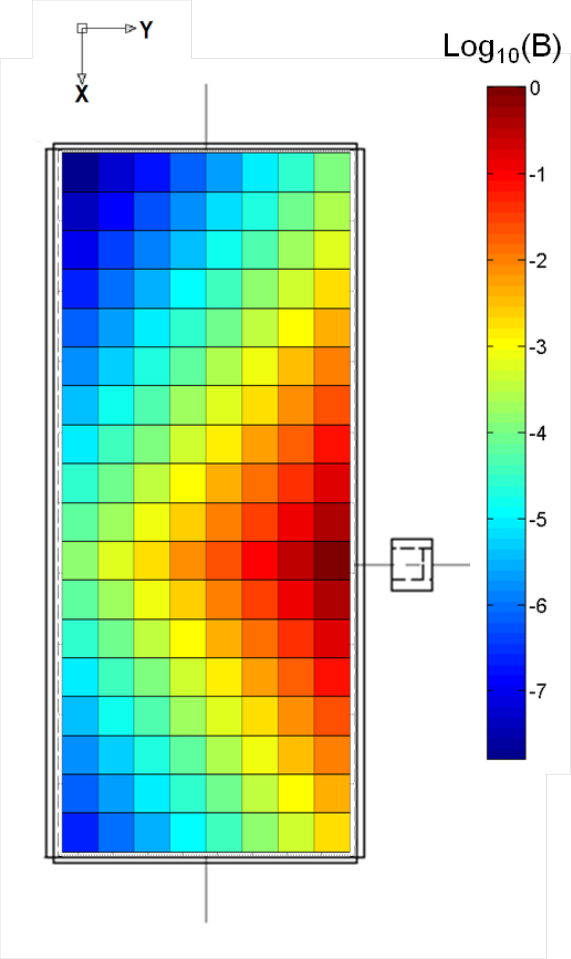

Figure 10: The source biasing parameters as a function of x and y overlayed on a schematic showing the detector location in Test Case II.

Test Case II Results					
	Analog	Trial 1	Trial 2	Trial 3	Trial 4
Source Biasing Dependence	none	none	x	x, y	x, y, z
MCNP5 Histories (N_{hist})	4427407358	697857695	442546144	375449347	375449347
Tally	5.2986E-10 ±4.18%	5.4020E-10 ±2.55%	4.8660E-10 ±1.46%	6.2733E-10 ±0.75%	6.2733E-10 ±0.75%
FOM	0.95 ±14.6%	2.6 ±23.7%	7.8 ±18.9%	30 ±8.2%	30 ±8.2%

Table 4: Results from MCNP5 runs of Test Case II with various degrees of source biasing sophistication

rejection sampling. (See Section 1.3.1.) The FOM is still expected to be valid, since the relative error and runtime are unaffected by the MCNP5 problem that distorts the tally mean.

Also note that the MCNP5 random number generator may overrun its period when more than 460 million histories are sampled. The results are not expected to be affected by the overrun, since random numbers are used in different ways in different histories [Hendricks 1991, MCNP 2008a, p. 2-195].

4 Conclusions

4.1 Introduction

This chapter will discuss the results presented in Section 3. Test Case I suggests that the FOM is greatly reduced by weight windows that do not monotonically decrease along paths away from the source, even if the weight windows are derived from an adjoint solution that is physically accurate. The results from Test Case II demonstrate the necessity of source biasing in problems where the importance function varies greatly over the source domain. Finally, the false-convergence problem observed in Test Case I suggests that other hybrid methods (such as LIFT) may be better suited for strongly angle-dependent problems.

4.2 Smoothness of Weight Windows

Results in Section 3.3 indicate that non-monotonicity of the weight windows along frequently sampled paths will reduce the FOM. This non-monotonicity may be caused by a poor deterministic solution (as in Section 3.3.1) or by the characteristics of the problem (as in Section 3.3.2).

This finding is reasonable: consider histories traveling from a region of low importance toward a region of high importance. If the weight window smoothly decreases from 1 to 0.5, each history will split into two. If the weight window increases from 1 to 2 before decreasing to 0.5, half of the histories will be terminated, while the surviving half will be split four-fold. Although the computational cost is slightly reduced by terminating half of the histories, most of the cost is still

incurred because the surviving histories are split four-fold. Because the four-fold split histories are all at the same position in P, the covariance of their detector responses is much higher than the covariance of responses among two sets of two-fold split histories. Therefore in the non-monotonic case, the overall solution variance is increased, with trivial reduction of the CPU cost.

4.3 Advantage of CADIS

Results in Section 3.5 support prior work that an explicit source biasing technique (such as CADIS) is an important improvement in Monte Carlo simulation. One can even defend a process in which source biasing is a consideration for any simulation using weight windowing.

This paradigm suggests that CADIS-like source biasing capability should be included more often in weight-windowing codes. For example, Attila^{TM} has features designed to generate weight windows, but no capability to create a complementing source definition. MCNP5 can read externally generated weight windows, but cannot automatically generate a volumetric source that is biased to complement the weight windows. Automatic source biasing features would be an important step toward a fully automated hybrid method.

4.4 Comparison of Adjoint-Derived Weight Windowing with Alternative Methods

False convergence is an over-estimation of the Monte Carlo solution's precision due to under-sampling of photon paths which contribute significantly to the mean.

Weight windowing can significantly improve the FOM for heavily shielded problems, but may increase the frequency of false convergence when large streaming regions exist near the detector. For example, Test Case I has a streaming region near the detector. In that case, regions of phase space near the concrete slab were significantly undersampled, leading to false convergence. The LIFT method may prove to be a more reliable hybrid method for problems where the adjoint function varies strongly with angle, such as Test Case I.

Ideally, a variance reduction method re-distributes the Monte Carlo histories to resemble the contributon flux. In the limit as the weight window mesh becomes infinitely fine; the frequency of weight window application approaches infinity; and window width approaches zero, the history flux will approach the contributon flux. In that limit, adjoint-derived weight windowing is similar to LIFT. The difference between these approaches is that weight windowing is an inherently reactive method; only once a history reaches an important region of P is it split or rouletted to match the contributon flux. By design, the LIFT method modifies the transport operator, actively channeling histories into important regions of P.

Consider histories in Test Case I as they leave the shielding or concrete regions and enter the air with a free path to the detector. Any splitting that occurs in the free-streaming region is irrelevant, since each split photon would contribute identically to the tally. The last effective weight windowing event therefore occurs before the history enters the streaming region. Since the adjoint function decreases as $1/r^2$ in the streaming region, where r is the distance from the detector, it is reasonable to make the following estimation: a history whose last effective weight windowing event occured at distance r from the detector will contribute an expected amount proportional to r^2 to the tally with probability $1/r^2$. When the

rare history scatters from a large distance r to the detector, the large contribution to the tally significantly increases the estimated solution variance. This increase in solution variance indicates that the path described is undersampled and the solution precision was overestimated prior to this history.

The LIFT method's "proactive" re-distribution of histories avoids this false convergence by biasing the scattering kernel. When histories approach the streaming region near the detector, LIFT preferentially scatters the histories in the direction of the detector; therefore, many histories with reduced weight reach the detector. If the adjoint solution were perfectly known and LIFT were perfectly applied, every history would reach the detector and contribute identically; LIFT therefore approximates a zero-variance method, while weight windowing cannot. [Turner 1997a]

5 Future Work

5.1 Introduction

This chapter presents several ideas that may be useful for improving the simulation of nonproliferation problems or hybrid simulation in general.

Test Case II is an example of a problem in which the energy distribution of the detector response is useful for discriminating between fissile and non-fissile isotopes. Although the FW-CADIS method has been used to balance the adjoint source of two or more detectors in space, the method could be extended to improve the simulation of the energy response distribution of a single energy-sensitive detector. The use of FW-CADIS in spectrography problems is discussed in Section 5.2.

In most hybrid methods, the adjoint solution is simplified in space or direction when generating weight windows. A rigorous method has not been presented for simplifying the adjoint solution. Section 5.3 presents a new method for the simplification of the adjoint solution derived from neutronic cross section homogenization theory.

The codes used in this thesis were designed to generate weight windows, but could not automatically generate a complementing source biasing distribution. Section 5.4 suggests a new method to easily match a volumetric source distribution to weight windows. This method would require rejection sampling and source biasing to be simultaneously used, which is likely to produce inaccurate results. A new type of tally is presented to correct the inaccuracy that arises when source biasing is used with rejection sampling.

5.2 Use of FW-CADIS for Energy-Dependent Source-Detector Problems

In many non-destructive assay problems similar to Test Case II, spectral information from the detector is key in assessing the quantities of interest. When one region of the spectrum has a relatively low flux, the FOM for the corresponding energy bin will be lower than for bins in other regions of the spectrum.

In problems where multiple detectors respond to photons in different regions of phase space, the FW-CADIS method offers a way to balance the adjoint source strength of the detectors so that their Monte Carlo response estimates converge at similar rates. This tool has been applied to problems with detectors at different spatial locations; it could be extended to problems where detectors exist at the same spatial location but respond differently to photons of different energies (i.e., the energy bins of a spectral detector).

5.3 An Improved Simplification Scheme for Weight Windows Generation

The adjoint solution is often simplified in space and angle as it is converted to weight windows. When the forward and adjoint fluxes vary widely within the homogenized region, care should be taken to use the most relevant adjoint information when simplifying the adjoint function.

For example, consider regions near the air/concrete interface of Test Case I. Attila^{TM} simplifies the adjoint solution in space by averaging the solutions at the eight vertices of the weight window cell. Because the importance of photons is so low below the concrete interface, the weight window for the cell will be set very

high. Setting the weight window high for this cell is not appropriate, since most of the photons simulated in this cell will be above the concrete.

As another example, consider the active interrogation problem described in [Peplow 2010]. A narrow neutron beam is directed through air to a distant interrogation target, i.e., Fig. 11. For a region of the problem far from the target, the

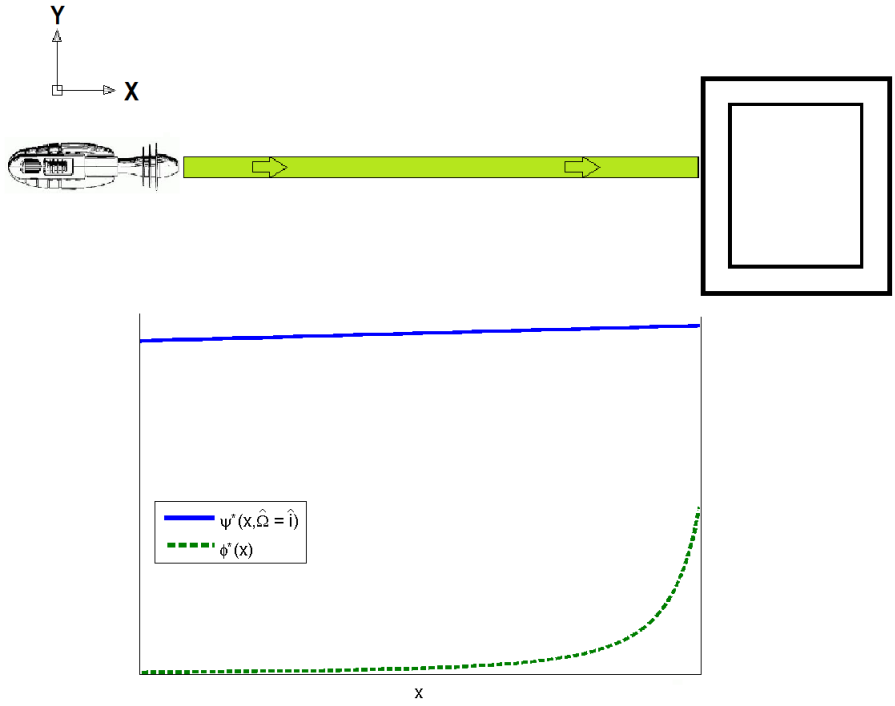

Figure 11: In the distant interrogation problem, a neutron beam (green) is incident upon a target of interest (right). The scalar adjoint flux Φ^* changes much more rapidly than the adjoint flux in the beam direction, $\Psi^*(\hat{\Omega} = \hat{i})$.

importance of photons traveling in *all* directions is proportional to $1/r^2$ where r is the distance from the region to the target. Intuitively, however, the importance of neutrons in the beam increases very little as they stream toward the target, since all neutrons in the beam are likely to reach the target. Since simulation of this problem is "not always helped by traditional space/energy CADIS," Peplow solved

it using anisotropic weight windows, i.e., by making fewer simplifications to the adjoint solution [Peplow 2010]. Peplow's method suggests that the information in the anisotropic adjoint solution should not be represented isotropically by simply integrating ψ^* over all angles.

The task of simplifying the adjoint flux is conceptually similar to the spatial homogenization of cross sections in reactor analysis. The best practices in reactor analysis are intended to conserve the reaction rate within the cell. In other words, the reaction rate

$$RR = \int_{CV} \Phi(\vec{x})\ \Sigma(\vec{x})\ dV = \overline{\Sigma} \int_{CV} \Phi(\vec{x})\ dV \tag{17}$$

where CV is the control volume which contains multiple materials, $\Sigma(\vec{x})$ is the reaction cross section of interest, and $\overline{\Sigma}$ is the homogenized cross section.

A similar concept could be applied to the simplification of the adjoint function for use in weight windows. Accounting for the distribution of photons throughout the cell (i.e., the forward flux), the expected contribution of photons in the phase control volume CV is

$$\overline{\Psi^*} = \frac{\int_{CV} \Psi(P)\ \Psi^*(P)\ dP}{\int_{CV} \Psi(P)\ dP} \tag{18}$$

Weight windows derived from $\overline{\Psi^*}$ would be most appropriate for simulating Ψ.

5.4 Extending the CADIS Source Distribution to Volumetric Sources in MCNP5

In many problems, such as Test Case II, the source domain is not a simple function of space. For these cases it is often effective to sample from a simple superset of the domain, then reject and re-sample any values that fall outside the domain. The "rejection" sampling method could even automate the process of

creating a volumetric source with biasing parameters derived to perfectly match the weight windows distribution: appropriate regions of the weight window distribution could form a superset of the source domain, and the sampling routine could bias the source toward regions with low weight windows. (A^3MCNP and ADVANTG employ a similar method by representing volumetric sources as a series of points from which to sample.)

Unfortunately, MCNP5 may produce biased results if source biasing is used with rejection sampling [MCNP 2008b p. 3-59]. Based on the source biasing parameters, the MCNP5 code automatically adjusts and normalizes the histories' birth weight assuming that none are rejected. If a larger fraction high-weight histories are accepted than low-weight histories, the mean weight of histories will be higher than expected. (See Section 1.3.1.) Tally results are proportional to the mean birth weight.

To effectively use source biasing with rejection sampling, a correction for the unfairly biased mean birth weight must be applied. To find the correction factor, an "F0" tally could be used to find the mean birth weight of histories. Implementing such a feature in MCNP5 would give users important information about the simulation's accuracy and grant them greater flexibility in their source definition.

Bibliography

[Attila 2009] "Attila User's Manual, Chapter 2." *Attila Help System:* Transpire, Inc., 2009.

[Baker 1993] Baker, R. S. "Hybrid S_N/Monte Carlo Research and Results." *Advanced Monte Carlo Computer Programs for Radiation Transport.* DOE Information Bridge, 1993.

[Barrett 2001] Barrett, C. L., and E. W. Larsen. "A Variationally-Based Variance Reduction Method for Monte Carlo Neutron Transport Calculations." *Annals of Nuclear Energy* 28 (2001): 457-75.

[Becker 2007] Becker, T. L., A. B. Wollaber, and E. W. Larsen. "A Hybrid Monte Carlo-Deterministic Method for Global Particle Transport Calculations." *Nuclear Science and Engineering* 155 (2007): 155-67.

[Booth 1983] Booth, T. E. "Weight Window / Importance Generator for Monte Carlo Streaming Problems." *Sixth International Conference on Radiation Shielding.* Los Alamos National Laboratory, 1983.

[Booth 1984] Booth, T. E., and J. S. Hendricks. "Importance Estimation in Forward Monte Carlo Calculations." *Nuclear Technology / Fusion* 5.1 (1984): 90-100.

[Booth 1985] Booth, T. E. *A Sample Problem for Variance Reduction in MCNP* . Los Alamos, NM: Los Alamos National Laboratory, 1985.

[Booth 2010] Booth, T. E. "Intuition and Variance Reduction in Monte Carlo Simulations." *Topical Meeting of the Radiation Protection and Shielding Division of the American Nuclear Society* . Los Alamos National Laboratory, Los Vegas, NV, 2010.

[Burn 1995] Burn, K.W. "Extending the Direct Statistical Approach to Include Particle Bifurcation between the Splitting Surfaces." *Nuclear Science and Engineering* 119 (1995): 44-79.

[Chucas 1994] Chucas, S., and M. Grimstone. "The Acceleration Techniques Used in the Monte Carlo Code Mcbend." *8th Interantional Conference on Radiation Shielding.* The ANSWERS Software Service, 1994.

[Coveyou 1967] Coveyou, R. R., V. R. Cain, and K. J. Yost. "Adjoint and Importance in Monte Carlo Application." *Nuclear Science and Engineering* 27 (1967): 219-34.

[Densmore 2002] Densmore, J. D. "Variational Variance Reduction for Monte Carlo Reactor Analysis." University of Michigan, 2002.

[Densmore 2004] Densmore, J. D., and E. W. Larsen. "Variational Variance Reduction for Monte Carlo Eigenvalue and Eigenfunction Problems." *Nuclear Science and Engineering* 146.2 (2004): 121-40.

[Densmore 2008] Densmore, J. D., T. M. Evans, and M. W. Buksas." A Hybrid Transport-Diffusion Algorithm for Monte Carlo Radiation-Transport Simulations on Adaptive Refinement Meshes in Xy Geometry." *Nuclear Science and Engineering* 159.1 (2008): 1-22.

[Garcia-Pareja 2007] Garcia-Pareja, S., M. Vilches, and A. M. Lallena. "Ant Colony Method to Control Variance Reduction Techniques in the Monte Carlo Simulation of Clinical Electron Linear Accelerators." *Nuclear Instruments and Methods in Physics Research A* 580 (2007): 510-13.

[Gardner 1999] Gardner, R. P., and L. Liu. "Monte Carlo Simulation of Neutron Porosity Oil Well Logging Tools: Combining the Geometry-Independent Fine-Mesh Importance Map and One-Dimensional Diffusion Model Approaches." *Nuclear Science and Engineering* 133.1 (1999): 80-91.

[Geant4 2010] "Geant4 User Documentation". 2010. <http://geant4.web.cern.ch/geant4/support/userdocuments.shtml>. Geant4 International Collaboration. 4/14/2011 2011.

[Haghighat 2003] Haghighat, A., and J. C. Wagner. "Monte Carlo Variance Reduction with Deterministic Importance Functions." *Progress in Nuclear Energy* 42.1 (2003): 25-53.

[Hendricks 1991] Hendricks, J. S. "Effects of Changing the Random Number Stride in Monte Carlo Calculations." *Nuclear Science and Engineering* 109.1 (1991): 86-91.

[Hendricks 2000] Hendricks, J. S., and C. N. Culbertson. "An Assessment of MCNP Weight Windows." *American Nuclear Society PHYSOR 2000 Conference.* 2000.

[Hoogenboom 2008] Hoogenboom, J. Eduard. "Zero-Variance Monte Carlo Schemes Revisited." *Nuclear Science and Engineering* 160 (2008): 1-22.

[Liu 1997] Liu, L., and R. P. Gardner. "A Geometry-Independent Fine-Mesh-Based Monte Carlo Importance Generator." *Nuclear Science and Engineering* 125.2 (1997): 188-95.

[MCNP 2008a] *MCNP — A General Monte Carlo N-Particle Transport Code, Version 5, Vol. I: Overview and Theory.* Los Alamos, NM: Los Alamos National Laboratory, 2008.

[MCNP 2008b] *MCNP — A General Monte Carlo N-Particle Transport Code, Version 5, Vol. II: User's Guide.* Los Alamos, NM: Los Alamos National Laboratory, 2008.

[Mickael 1995] Mickael, M. W. "A Fast, Automated, Semideterministic Weight Windows Generator for MCNP." *Nuclear Science and Engineering* 119.1 (1995): 34-43.

[Miller 2010] Miller, E. A., et al. "Scatter in Cargo Radiography." *Applied Radiation and Isotopes* (2010).

[Mosher 2009] Mosher, S. W., et al. "Automated Weight-Window Generation for Threat Detection Applications Using ADVANTG." *International Conference on Mathematics, Computational Methods & Reactor Physics.* American Nuclear Society, 2009.

[Mosher 2010a] Mosher, S. W. "A New Version of the ADVANTG Variance Reduction Generator." *RPSD 2010 Topical Meeting* . 2010.

[Mosher 2010b] Mosher, S. W., J. C. Wagner, and D. E. Peplow. "Information About ADVANTG." Ed. Bevill, Aaron. An email exchange regarding the current capabilities of ADVANTG, especially volumetric source distributions. ed. Oak Ridge, TN, 2010.

[NEA 2008] "NEA-1716 Tripoli-4.3.3 & 4.4". Issy-les-Moulineaux, France, 2008. *Data Bank: Computer Program Services.* TRIPOLI-4.3.3 & 4.4, Coupled Neutron, Photon, Electron, Positron 3-D, Time Dependent Monte-Carlo, Transport Calculation. Nuclear Energy Agency. Oct. 4 2010.

[Nouri 1999] Nouri, Ali, et al. *MORET4: A Versatile and Accurate Monte-Carlo Code for Criticality Calculations.* France: ISPN, 1999.

[Painter 1980] Painter, J. W., S. A. W. Gerstl, and G. C. Pomraning. *Theory of Contributon Transport.* Los Alamos, NM: Los Alamos National Laboratory, 1980.

[Peplow 2006] Peplow, D. E., et al. "MONACO/MAVRIC: Computational Resources for Radiation Protection and Shielding in Scale." *American Nuclear Society 2006 Winter Meeting.* 2006.

[Peplow 2007] Peplow, D. E., E. D. Blakeman, and J. C. Wagner. "Advanced Variance Reduction Strategies for Optimizing Mesh Tallies in MAVRIC." *American Nuclear Society 2007 Winter Meeting.* 2007.

[Peplow 2010] Peplow, D. E., S. W. Mosher, and T. M. Evans. "Hybrid Monte Carlo/Deterministic Methods for Streaming/Beam Problems." *American Nuclear Society Joint Topical Meeting of the Radiation Protection and Shielding Division.* Oak Ridge National Laboratory, 2010.

[Seydaliev 2008] Seydaliev, Marat, and D.L. Henderson. *Contributon Theory for Shielding Analysis.* Madison, WI: Fusion Technology Institute (University of Wisconsin), 2008.

[Sheu 2008] Sheu, R. J., et al. "Shielding Calculations for a Spent Fuel Storage Cask: A Comparison of Discrete Ordinates, Monte Carlo, and Hybrid Methods." *Nuclear Science and Engineering* 159 (2008): 23-36.

[Shuttleworth 2000] Shuttleworth, T., M. Grimstone, and S. Chucas. "Application of Acceleration Techniques in Mcbend." Ninth International Conference on Radiation Shielding. 2000. *Journal of Nuclear Science and Technology.*

[Smith 2005] Smith, H. P., and J. C. Wagner. "A Case Study in Manual and Automated Monte Carlo Variance Reduction with a Deep Penetration Reactor Shielding Problem." *Nuclear Science and Engineering* 149 (2005): 23-37.

[Smith 2008] Smith, L. E., et al. "Coupling Deterministic and Monte Carlo Transport Methods for the Simulation of Gamma-Ray Spectroscopy Scenarios." *IEEE Nuclear Science Symposium 2006* 55.5 (2008): 2598-606.

[Sweezy 2005] Sweezy, J., et al. "Automated Variance Reduction for MCNP Using Deterministic Methods." *Radiation Protection Dosimetry* 116.1-4 (2005): 508-12.

[Tang 1998] Tang, J. S. *SAS4: A Monte Carlo Cask Shielding Analysis Module Using an Automated Biasing Procedure.* Washington, DC: Office of Nuclear Material Safety and Safeguards (US NRC), 1998.

[Turner 1997a] Turner, S. A., and E. W. Larsen. "Automatic Variance Reduction for Three-Dimensional Monte Carrlo Simulations by the Local Importance Function Transform – I: Analysis." *Nuclear Science and Engineering* 127 (1997): 22-35.

[Turner 1997b] Turner, S. A., and E. W. Larsen. "Automatic Variance Reduction for Three-Dimensional Monte Carrlo Simulations by the Local Importance Function Transform – II: Numerical Results." *Nuclear Science and Engineering* 127 (1997): 36-53.

[Van Riper 1997] Van Riper, K. A., et al. "Avatar – Automatic Variance Reduction in Monte Carlo Calculations." *Joint International Conference on Mathematical Methods and Supercomputing in Nuclear Applications.* Los Alamos National Laboratory, 1997.

[Wagner 1998] Wagner, J. C., and A. Haghighat. "Automated Variance Reduction of Monte Carlo Shielding Calculations Using the Discrete Ordinates Adjoint Function." *Nuclear Science and Engineering* 128 (1998): 186-208.

[Wagner 2000] Wagner, J. C., and A. Haghighat. "A^{3}MCNP: Automatic Adjoint Accelerated MCNP User's Manual." *Computational Medical Physics Working Group II Meeting Workshops.* 1.0i ed. Gainesville, FL: American Nuclear Society, 2000.

[Wagner 2002] Wagner, J. C. "An Automated Deterministic Variance Reduction Generator for Monte Carlo Shielding Applications." *American Nuclear Society / Radiation Protection & Shielding Division 12th Biennial RPSD Topical Meeting.* 2002.

[Wagner 2007] Wagner, J. C., E. D. Blakeman, and D. E. Peplow. "Forward-Weighted CADIS Method for Global Variance Reduction." *American Nuclear Society 2007 Winter Meeting.* 2007.

[Wagner 2009] Wagner, J. C., D. E. Peplow, and T. M. Evans. "Automated Variance Reduction Applied to Nuclear Well-Logging Problems." *Transactions of the American Nuclear Society* 99 (2009): 566-69.

[Wareing 2001] Wareing, T. A., et al. "Discontinuous Finite Element S_n Methods on Three-Dimensional Unstructured Grids." *Nuclear Science and Engineering* 138.2 (2001).

[Williams 1991] Williams, M. L. "Generalized Contributon Response Theory." *Nuclear Science and Engineering* 108.4 (1991): 355-83.

APPENDICES

Appendix A Test Case I Specifications

Test Case I Adjoint Calculation Settings, Part 1	
Parameter	Value
Calculation Type	Steady State
Transport Operator	Adjoint
Global Mesh Size	30 cm
Nodes	2136
Sides	1662
Cells	10963
Transport Correction	None
Few-group Structure (keV)	400.000 – 334.348 334.348 – 293.790 293.790 – 239.366 239.366 – 170.673 170.673 – 25.000
Volume source	no volume source
boundary values	vacuum
FSDS Ray Trace Formulation	Geometric (dot product)
Point Source Visualization	no
Skip Merge Step	no
Point Source Position	$< 51.25, 0, 51 >$
Ray Tracing Style	Trace to Quadrature Points
Intensity	1
Minimum Radius	0.0001
Source Spectrum Particle	Gamma
Spectrum Type	Constant
Conserve	Particles
Spectrum	$\chi = 1$ for each energy bin

Table 5: Problem, mesh, cross section, source, and boundary value settings used in the deterministic simulation to generate adjoint flux moments

Test Case I Adjoint Calculation Settings, Part 2	
Parameter	Value
Quadrature	Triangular Chebychev Legendre
SN Order	4
Scattering Treatment	Galerkin
Scattering Degree	1
Maximum Runtime	3276.7 hours
Maximum Outer Iterations	1
Maximum Inner Iterations	100
Convergence Criterion	1.00E-04
Memory Strategy	High Speed
Sweep Data Strategy	High Speed
Advanced Options	no
Write Terminal Restart File	yes
Terminal Restart Precision	single
Write Tecplot File	yes
Write GMV File	no
Include Default Visualization Data	yes
Hours Between Contingency Restart File Writes:	0
Weight Windows Input Generator Enabled	no
Enable Activation?	no

Table 6: Quadrature, convergence, and output settings used in the deterministic simulation to generate adjoint flux moments

Test Case I Adjoint Calculation Settings, Part 3	
Parameter	Value
Edit 1: Adjoint Scalar Flux at Source	
Active	yes
Type	Scalar Flux
Scale Factor	1
Response Function	none
Energy Groups	All
Spatial Set	Point at $< -57.75, 0, 53.5 >$
Extra Report Output	By Energy Group
Last Collided Option	no
Visualization File Output: Include Report Results	no
Edit 2: Adjoint Scalar Flux Along Path	
Active	yes
Type	Scalar Flux
Scale Factor	1
Response Function	none
Energy Groups	All
Spatial Set	Line: 50 points from $< -57.75, 0, 53.5 >$ to $< 51.25, 0, 51 >$
Extra Report Output	By Space and Energy
Last Collided Option	no
Visualization File Output: Include Report Results	no

Table 7: Extra reports used in the deterministic simulation gather information about the solution

Test Case I Weight Window Calculation Settings	
Parameter	Value
Volume Source	Region-wise Constant (soil)
Volume Source Spectrum	constant spectrum, multiplier 1e-12
Starting Flux File	corresponding adjoint calculation
Report Run Only	yes
Write Terminal Restart File	no
Write Tecplot File	no
Weight Windows Generator Enabled	yes
N_x	150
N_y	40
N_z	40
Normalization (C_{ww})	varies
Custom Reports	no custom report

Table 8: Settings used in the report-only Attila™ simulation to generate weight windows from adjoint flux moments

Test Case I MCNP5 Geometry
Cell Cards
101 1 -1.0 -101 $ Mulch
102 2 -0.433 -102 #101 $ Crate
103 3 -2.3 -103 $ Concrete Slab
104 4 -1.82 -104 $ Soil
105 5 -0.001205 -105 #101 #102 #500 $ Air
500 5 -0.001205 -106 $ Tally Volume
999 0 105 #101 #103 #104 $ Universe
Surface Cards
101 rpp -43.21 43.21 -58.46 58.46 5.08 99.04
102 rpp -45.75 45.75 -61.00 61.00 0.00 110.0
103 rpp -100.00 100.00 -100.00 100.00 -7.62 0.00
104 rpp -100.00 100.00 -100.00 100.00 -57.62 -7.62
105 rpp -100.00 100.00 -100.00 100.00 0.00 207.62
106 sph 51.25 0 51 1.0

Table 9: Geometry input cards for the MCNP5 simulation used in the mulch case

Test Case I MCNP5 Materials			
ID	***Material***	***Composition***	
M1	Mulch	hydrogen-1	5.7889 %
		carbon-12	48.2667 %
		oxygen-16	45.9444 %
M2	Crate	*same as "Mulch"*	
M3	Concrete	hydrogen-1	2.2101 %
		carbon-12	0.2484 %
		oxygen-16	57.4930 %
		sodium (natural)	1.5208 %
		magnesium (natural)	0.1266 %
		aluminum (natural)	1.9953 %
		silicon (natural)	30.4627 %
		potassium (natural)	1.0045 %
		calcium (natural)	4.2951 %
		iron (natural)	0.6435 %
M4	Soil	hydrogen-1	0.1325 %
		carbon-12	0.0292 %
		oxygen-16	47.1188 %
		sodium (natural)	2.8817 %
		magnesium (natural)	2.1296 %
		aluminum (natural)	8.2089 %
		silicon (natural)	28.0267 %
		potassium (natural)	2.6407 %
		calcium (natural)	3.6824 %
M5	Air	carbon-12	0.0124 %
		nitrogen (natural)	75.5268 %
		oxygen-16	23.1781 %
		argon (natural)	1.2827 %

Table 10: Material compositions used in the MCNP5 model of the mulch case, expressed in weight percent

Test Case I Source Distribution		
Lower Bound [MeV]	***Upper Bound*** [MeV]	***Rel. Strength***
0	0.0038	8.81E-04
0.0038	0.0041	4.03E-04
0.0041	0.0043	2.43E-02
0.0043	0.0047	2.37E-02
0.0047	0.0054	3.31E-03
0.0054	0.0306	1.29E-01
0.0306	0.031	2.39E-01
0.031	0.035	6.53E-02
0.035	0.036	1.60E-02
0.036	0.0531	7.88E-03
0.0531	0.0796	1.16E-02
0.0796	0.081	1.24E-01
0.081	0.1606	2.17E-03
0.1606	0.2232	1.67E-03
0.2232	0.2764	2.57E-02
0.2764	0.3029	6.68E-02
0.3029	0.356	2.26E-01
0.356	0.3838	3.24E-02

Table 11: Histogram energy distribution for the mulch case

Appendix B Test Case II Specifications

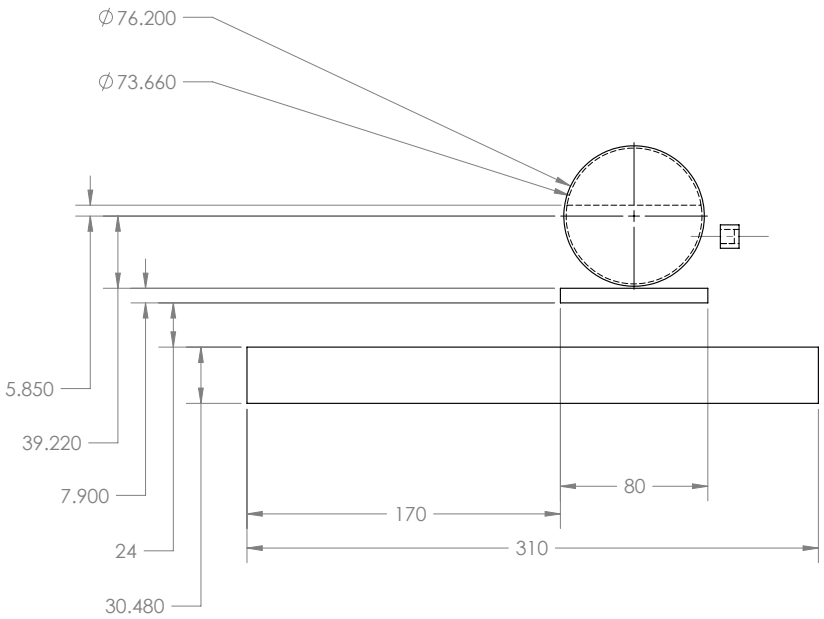

Figure 12: The front view of Test Case II shows the large (diameter 76.2 cm) UF_6 cylinder, small cylindrical detector (at right), a metal slab representing a cart (center), and a large concrete slab (bottom). The UF_6 cylinder is partly emptied.

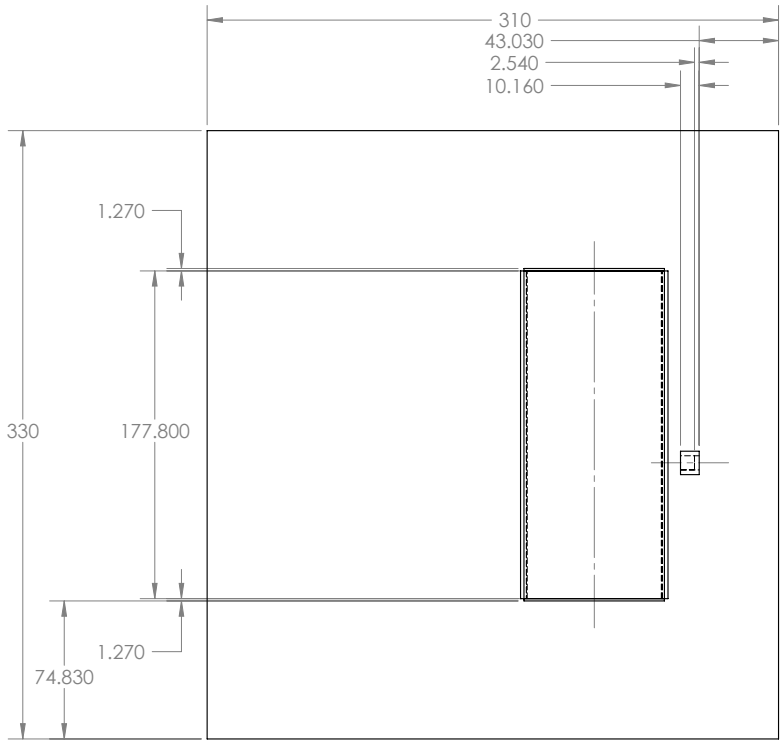

Figure 13: The top view of Test Case II shows the large UF_6 cylinder and small detector suspended above the concrete slab. The cart is mostly concealed by the UF_6 cylinder.

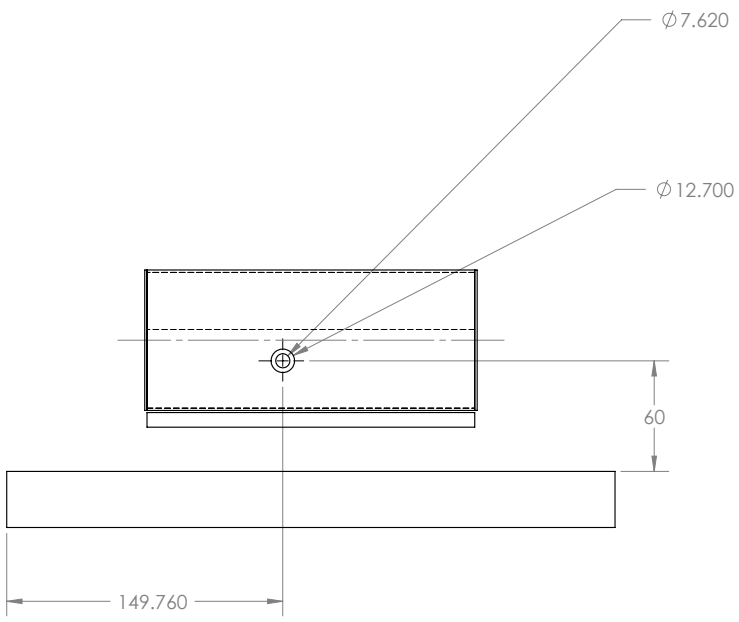

Figure 14: The side view of Test Case II shows the small (diameter 12.7 cm) detector in front of the UF_6 cylinder. Below the cylinder are the cart and concrete slab.

Test Case II Adjoint Calculation Settings, Part 1	
Parameter	Value
Calculation Type	Steady State
Transport Operator	Adjoint
Global Mesh Size	100 cm
Nodes	17594
Sides	8749
Cells	102225
Transport Correction	Diagonal
Few-group Structure (MeV)	2.14182 – 1.40561 1.40561 – 0.800770 0.800770 – 0.341016 0.341016 – 0.050000
Volume source	no volume source
boundary values	vacuum
FSDS Ray Trace Formulation	Geometric (dot product)
Point Source Visualization	no
Skip Merge Step	no
Point Source Position	$< 15.24, 46.81, 60 >$
Ray Tracing Style	Trace to Quadrature Points
Intensity	1
Minimum Radius	0.0001
Source Spectrum Particle	Gamma
Spectrum Type	Constant
Conserve	Particles
Spectrum	$\chi = 1$ for each energy bin

Table 12: Problem, mesh, cross section, source and boundary value settings used in the Attila^{TM} FSDS run to generate adjoint flux moments

Test Case II Adjoint Calculation Settings, Part 2	
Parameter	Value
Quadrature	Triangular Chebychev Legendre
SN Order	8
Scattering Treatment	Galerkin
Scattering Degree	2
Maximum Runtime	3276.7 hours
Maximum Outer Iterations	1
Maximum Inner Iterations	100
Convergence Criterion	1.00E-04
Memory Strategy	Low Memory
Sweep Data Strategy	High Speed
Advanced Options	no
Write Terminal Restart File	yes
Terminal Restart Precision	single
Write Tecplot File	yes
Write GMV File	no
Include Default Visualization Data	yes
Hours Between Contingency Restart File Writes:	0
Weight Windows Input Generator Enabled	no
Enable Activation?	no

Table 13: Quadrature, convergence, and output settings used in the Attila™ FSDS run to generate adjoint flux moments

Test Case II Weight Window Calculation Settings	
Parameter	Value
Volume Source	Region-wise Constant (NaI)
Volume Source Spectrum	constant spectrum, multiplier 1e-12
Write Terminal Restart File	no
Write Tecplot File	no
Weight Windows Generator Enabled	yes
N_x	32
N_y	24
N_z	12
Normalization (C_{ww})	10^{-2}
Custom Reports	no custom report

Table 14: Settings used in the report-only Attila^{TM} run to generate weight windows from adjoint flux moments

Test Case II MCNP5 Cells, Part 1	
Detector 1	
NaI Crystal	210 2000 -3.76 -210
ID of inner sleeve	211 9100 -0.001205 -211 210
OD of inner sleeve	212 2100 -2.7 -212 211
ID of outer sleeve	213 9200 -11.4 -213 212
OD of outer sleeve	214 2100 -2.7 -214 213
Detector 2	
LaBr Crystal	220 2300 -5.06 -220
ID of inner sleeve	221 9100 -0.001205 -221 220
OD of inner sleeve	222 2100 -2.7 -222 221
ID of outer sleeve	223 9200 -11.4 -223 222
OD of outer sleeve	224 2100 -2.7 -224 223
Detector 3	
NaI Crystal	230 2000 -3.76 -230
ID of inner sleeve	231 9100 -0.001205 -231 230
OD of inner sleeve	232 2100 -2.7 -232 231
ID of outer sleeve	233 9200 -11.4 -233 232
OD of outer sleeve	234 2100 -2.7 -234 233
Detector 4	
LaBr Crystal	240 2300 -5.06 -240
ID of inner sleeve	241 9100 -0.001205 -241 240
OD of inner sleeve	242 2100 -2.7 -242 241
ID of outer sleeve	243 9200 -11.4 -243 242
OD of outer sleeve	244 2100 -2.7 -244 243
Neutron Detector	
Outside Neutron Shielding Box (Borated Poly)	260 4200 -1.08 261 -260
Neutron Shielding Box (Poly)	261 4100 -0.93 -262 #262 #263 #264 #265
He-3 Neutron Detector 1	262 4000 -4.85E-4 -263
He-3 Neutron Detector 2	263 4000 -4.85E-4 -264
He-3 Neutron Detector 3	264 4000 -4.85E-4 -265
He-3 Neutron Detector 4	265 4000 -4.85E-4 -266
Detector Electronics	266 2200 -0.96 -261 262
Spacing	
Bounding box	250 9100 -0.001205 -250 214 224 234 244 260

Table 15: Cell input cards for the MCNP5 simulation used in Test Case II — detectors

Test Case II MCNP5 Cells, Part 2	
UF_6 Cylinder	
Cylinder wall	8501 9410 -7.85 8001 -8002 8003 -8004
Support to sit on	8507 9410 -7.85 8002 -8065
Support to sit on	8508 9410 -7.85 8002 -8066
Cylinder wall left	8510 9410 -7.85 8006 -8005 -8001
Cylinder wall right	8511 9410 -7.85 8007 -8008 -8001
N_2 in cylinder	8520 9510 -8.933E-4 8005 -8007 -8001 8020
UF_6 in cylinder	8521 9500 -5.1 8005 -8007 -8001 -8020
Cart	
Cart	8529 9410 -7.85 -8029
Front Axle	8530 9410 -7.85 -8030
Back Axle	8531 9410 -7.85 -8031
Front right wheel	8532 9410 -7.85 -8036 8030
Front left wheel	8533 9410 -7.85 -8037 8030
Back right wheel	8534 9410 -7.85 -8038 8031
Back left wheel	8535 9410 -7.85 -8039 8031
World	
Concrete Floor	8603 9400 -2.3 -8103 8104 8105
Railings	8604 9410 -7.85 -8104
Railings	8605 9410 -7.85 -8105
Air Within World	
Air inside universe	8611 9100 -1.205E-3 -9999 8002 8065 8066 8029 8030 8031 8036 8037 8038 8039 8103 250
-x cylinder end	8612 9100 -1.205E-3 -9999 -8002 -8003
+x cylinder end	8613 9100 -1.205E-3 -9999 -8002 8004
-x cylinder endcap gap	8614 9100 -1.205E-3 -8001 8003 -8006
+x cylinder endcap gap	8615 9100 -1.205E-3 -8001 -8004 8008
Edge of Model's Universe	
Outside universe	9999 0 9999

Table 16: Cell input cards for the MCNP5 simulation used in Test Case II — all geometry except detectors

Test Case II MCNP5 Surfaces, Part 1	
Detector 1	
Crystal	210 211 rcc -45.72 0 0 0 0 7.62 3.81
ID of inner sleeve	211 211 rcc -45.72 0 0 0 0 10.16 4.1275
OD of inner sleeve	212 211 rcc -45.72 0 0 0 0 10.16 4.445
ID of outer sleeve	213 211 rcc -45.72 0 0 0 0 10.16 6.0325
OD of outer sleeve	214 211 rcc -45.72 0 0 0 0 10.16 6.35
Detector 2	
Crystal	220 211 rcc -15.24 0 0 0 0 7.62 3.81
ID of inner sleeve	221 211 rcc -15.24 0 0 0 0 10.16 4.1275
OD of inner sleeve	222 211 rcc -15.24 0 0 0 0 10.16 4.445
ID of outer sleeve	223 211 rcc -15.24 0 0 0 0 10.16 6.0325
OD of outer sleeve	224 211 rcc -15.24 0 0 0 0 10.16 6.35
Detector 3	
Crystal	230 211 rcc 15.24 0 0 0 0 7.62 3.81
ID of inner sleeve	231 211 rcc 15.24 0 0 0 0 10.16 4.1275
OD of inner sleeve	232 211 rcc 15.24 0 0 0 0 10.16 4.445
ID of outer sleeve	233 211 rcc 15.24 0 0 0 0 10.16 6.0325
OD of outer sleeve	234 211 rcc 15.24 0 0 0 0 10.16 6.35
Detector 4	
Crystal	240 211 rcc 45.72 0 0 0 0 7.62 3.81
ID of inner sleeve	241 211 rcc 45.72 0 0 0 0 10.16 4.1275
OD of inner sleeve	242 211 rcc 45.72 0 0 0 0 10.16 4.445
ID of outer sleeve	243 211 rcc 45.72 0 0 0 0 10.16 6.0325
OD of outer sleeve	244 211 rcc 45.72 0 0 0 0 10.16 6.35
Neutron Detector	
Outside Neutron Shielding Box (Borated Poly)	260 211 rpp -28.336875 28.336875 7 35.09875 -4 9.208
Inside Neutron Shielding Box (Borated Poly)	261 211 rpp -23.256875 23.256875 12.08 30.01875 1.08 4.128
Neutron Shielding Box (Poly)	262 211 rpp -23.145750 20.859750 12.08 29.86 1.1435 4.0645
He-3 neutron detector 1	263 211 rcc -15.24 16.144 2.604 30.48 0 0 1.3081
He-3 neutron detector 2	264 211 rcc -15.24 19.954 2.604 30.48 0 0 1.3081
He-3 neutron detector 3	265 211 rcc -15.24 23.764 2.604 30.48 0 0 1.3081
He-3 neutron detector 4	266 211 rcc -15.24 27.574 2.604 30.48 0 0 1.3081
Spacing	
Bounding box	250 211 rpp -55 55 -6.4 35.1 -4.1 10.2

Table 17: Surface input cards for the MCNP5 simulation used in Test Case II — detectors

Test Case II MCNP5 Surfaces, Part 2	
UF_6 Cylinder	
Inside Cylinder	8001 111 C/X 0 71.12 36.83
Outside Cylinder	8002 111 C/X 0 71.12 38.10
Left end of lip	8003 111 PX -109.22
Right end of lip	8004 111 PX 97.97
Inside - end cap	8005 111 PX -88.9
Outside - end cap	8006 111 PX -90.17
Inside + end cap	8007 111 PX 88.9
Outside + end cap	8008 111 PX 90.17
UF_6 Fill level	8020 111 PZ 76.97
Cart	
Cart	8029 111 RPP -88.9 88.9 -40 40 25.12 33.02
Front Axle	8030 111 RCC 78.73 -50 15.24 0 100 0 2.54
Back Axle	8031 111 RCC -78.73 -50 15.24 0 100 0 2.54
Front right wheel	8036 111 RCC 78.73 -50 15.24 0 9 0 15
Front left wheel	8037 111 RCC 78.73 41 15.24 0 9 0 15
Back right wheel	8038 111 RCC -78.73 -50 15.24 0 9 0 15
Back left wheel	8039 111 RCC -78.73 41 15.24 0 9 0 15
Support to sit on	8065 111 RPP 77.46 80 -51.435 51.435 33.02 54.61
Support to sit on	8066 111 RPP -80 -77.46 -51.435 51.435 33.02 54.61
World	
Concrete Floor	8103 RPP -165 165 -100 100 -30.48 0.0
Metal Railing	8104 RPP -150 -134.76 -100 100 -2.54 0.0
Metal Railing	8105 RPP 134.76 150 -100 100 -2.54 0.0
Edge of Model's Universe	
Universe Definition	9999 RPP -165 165 -210 100 -30.48 150

Table 18: Surface input cards for the MCNP5 simulation used in Test Case II — all geometry except detectors

Test Case II MCNP5 Materials			
ID	***Material***	***Composition***	
M2100	Aluminum	aluminum (natural)	100 %
M2000	NaI Scintillator	sodium-23	50 $^{a}/_{0}$
		iodine-127	50 $^{a}/_{0}$
M2200	Electronics	hydrogen-1	4.25 %
		carbon-12	45.75 %
		aluminum-27	50 %
M2300	LaBr Scintillator	lanthanum (natural)	25 $^{a}/_{0}$
		bromine (natural)	75 $^{a}/_{0}$
M4200	Borated Polyethlylene	hydrogen-1	63.3333 %
		carbon-12	31.6667 %
		boron-10	0.98 %
		boron-11	4.02 %
M4100	Polyethylene	hydrogen-1	66.6667 $^{a}/_{0}$
		carbon-12	33.3333 $^{a}/_{0}$
M4000	Helium-3	helium-3	100 %
M9100	Air	carbon-12	0.0124 %
		nitrogen-14	75.5267 %
		oxygen-16	23.1781 %
		argon (natural)	1.2827 %
M9200	Lead	lead (natural)	100 %
M9400	Concrete	hydrogen-1	1 %
		oxygen-16	53.2 %
		sodium-23	2.9 %
		aluminum-27	3.4 %
		silicon (natural)	33.7 %
		calcium (natural)	4.4 %
		iron (natural)	1.4 %
M9410	Steel	carbon (natural)	0.19 %
		manganese-55	0.718 %
		silicon (natural)	0.282 %
		sulfur (natural)	0.1028 %
		iron (natural)	98.7072 %
M9500	UF_6	uranium-234	0.016226 %
		uranium-235	2.0042 %
		uranium-236	0.012341 %
		uranium-238	65.579 %
		fluorine-19	23.388 %
M9510	Nitrogen filler	nitrogen-14	100 %

Table 19: Material compositions used in the MCNP5 model of the UF_6 case, expressed in weight percent (or atom percent, as denoted by $^{a}/_{0}$)

Test Case II Source Distribution, Part 1					
Energy [MeV]	***Rel. Strength***	***Energy*** [MeV]	***Rel. Strength***	***Energy*** [MeV]	***Rel. Strength***
0.0044	1.11E+04	0.019	2.36E+03	0.087	1.23E+03
0.0092	8.45E+07	0.0191	4.44E+08	0.0877	3.40E+03
0.01	2.50E+03	0.0191	1.56E+05	0.09	5.69E+08
0.0102	1.28E+08	0.0196	1.03E+10	0.09	1.59E+08
0.0109	8.85E+03	0.0198	1.26E+09	0.0909	5.53E+03
0.0111	2.14E+08	0.0198	1.83E+05	0.0923	6.55E+07
0.0111	2.99E+04	0.02	1.76E+03	0.0923	1.39E+03
0.0114	4.95E+08	0.0203	3.18E+03	0.0924	4.61E+05
0.0114	3.96E+04	0.0204	3.33E+03	0.0928	4.54E+05
0.0116	1.02E+03	0.0256	2.47E+09	0.0931	8.29E+06
0.0117	2.02E+03	0.0274	6.64E+04	0.0934	9.23E+08
0.0123	3.52E+03	0.0316	2.70E+06	0.0947	2.03E+04
0.0126	1.54E+05	0.0382	1.06E+03	0.0947	4.25E+03
0.013	3.64E+09	0.0411	5.07E+06	0.0947	1.76E+03
0.013	5.09E+05	0.042	6.76E+06	0.0959	1.06E+08
0.0133	8.25E+09	0.0428	9.80E+06	0.0959	2.25E+03
0.0133	6.62E+05	0.0441	1.18E+05	0.0962	1.45E+07
0.0133	3.05E+03	0.0464	1.48E+03	0.0984	3.26E+04
0.0136	1.68E+04	0.0496	1.18E+04	0.0984	6.83E+03
0.0136	1.16E+04	0.0501	1.73E+03	0.0993	2.03E+07
0.0141	2.63E+03	0.0512	3.38E+06	0.0999	1.30E+03
0.0143	1.93E+03	0.0542	2.54E+06	0.1023	6.90E+07
0.0144	2.52E+03	0.0586	8.11E+07	0.1026	2.00E+03
0.0145	3.69E+07	0.0629	3.25E+03	0.1037	1.06E+03
0.0145	1.41E+04	0.0633	6.44E+05	0.1054	3.34E+08
0.015	6.76E+07	0.0638	3.89E+06	0.1058	1.20E+06
0.015	8.34E+03	0.0643	3.38E+06	0.1066	2.87E+06
0.0152	4.36E+03	0.0685	9.63E+05	0.108	1.00E+03
0.0157	1.81E+05	0.0727	1.86E+07	0.1082	3.86E+07
0.0161	2.61E+09	0.0728	4.24E+07	0.109	1.11E+08
0.0162	7.00E+05	0.0739	2.64E+03	0.1092	2.54E+08
0.0164	2.71E+03	0.0739	1.85E+03	0.111	1.19E+04
0.0165	3.53E+03	0.074	7.21E+03	0.111	2.50E+03
0.0166	6.32E+09	0.075	1.01E+07	0.1119	1.29E+07
0.0166	7.41E+05	0.0811	2.99E+03	0.1128	4.09E+04
0.0171	1.56E+04	0.0812	1.52E+08	0.1149	4.01E+03
0.0171	1.42E+04	0.0821	8.32E+07	0.1156	1.69E+05
0.0172	3.68E+07	0.0833	1.19E+04	0.1161	1.18E+07
0.0181	2.79E+07	0.0838	4.97E+03	0.1168	3.50E+06
0.0186	4.19E+04	0.0842	1.12E+09	0.12	4.39E+06

Table 20: Line energy spectrum of uranium-235 below 0.12 MeV

Test Case II Source Distribution, Part 2					
Energy [MeV]	***Rel. Strength***	***Energy*** [MeV]	***Rel. Strength***	***Energy*** [MeV]	***Rel. Strength***
0.1249	9.43E+06	0.2409	1.15E+07	0.4017	1.31E+03
0.1313	5.41E+03	0.2425	1.42E+05	0.4103	5.07E+05
0.134	4.06E+06	0.2469	1.01E+07	0.4484	1.69E+05
0.1357	1.32E+07	0.2496	1.32E+05	0.4551	1.35E+06
0.1367	2.03E+06	0.2504	1.10E+05	0.5172	6.76E+04
0.1367	7.10E+05	0.2562	1.37E+03	0.5695	2.89E+03
0.1405	1.20E+05	0.2582	9.59E+03	0.6988	1.24E+03
0.1408	3.72E+07	0.2603	1.30E+03	0.7332	2.33E+03
0.1438	1.78E+09	0.2665	1.01E+06	0.7409	1.20E+03
0.1451	9.80E+05	0.2676	1.96E+05	0.7425	6.76E+04
0.1459	5.41E+06	0.2694	2.68E+03	0.7428	9.55E+03
0.151	1.28E+07	0.2711	1.95E+03	0.7664	3.49E+04
0.1527	1.81E+03	0.2741	5.07E+03	0.7863	5.78E+03
0.1542	1.10E+03	0.2755	8.28E+06	0.7947	1.01E+05
0.1631	2.62E+07	0.2814	1.01E+06	0.7953	1.03E+03
0.1634	7.94E+08	0.283	8.45E+05	0.8099	8.61E+04
0.165	6.59E+05	0.2837	1.14E+04	0.8258	1.08E+03
0.1696	2.03E+05	0.2896	1.18E+06	0.8314	1.49E+03
0.1723	1.69E+06	0.2917	5.07E+05	0.8763	1.08E+03
0.1742	3.10E+06	0.2939	1.06E+03	0.8805	2.43E+03
0.1825	6.76E+07	0.3001	1.70E+04	0.8805	1.08E+03
0.1835	5.56E+06	0.3017	8.45E+05	0.8832	3.26E+03
0.1848	2.02E+03	0.3026	4.57E+03	0.8986	1.11E+03
0.1857	8.98E+09	0.3027	1.22E+04	0.922	1.40E+03
0.1888	5.41E+05	0.3087	6.59E+04	0.9257	2.97E+03
0.1927	1.44E+03	0.3107	6.76E+05	0.9267	2.43E+03
0.195	9.97E+07	0.311	4.90E+05	0.946	2.20E+03
0.1989	6.75E+06	0.3171	1.69E+05	0.946	1.21E+03
0.2021	1.69E+08	0.3179	1.35E+04	0.948	2.16E+03
0.2053	7.94E+08	0.3202	1.86E+04	1.001	1.10E+05
0.2153	4.56E+06	0.3301	9.38E+03	1.1937	1.52E+03
0.2179	6.76E+06	0.3409	1.24E+03	1.5101	1.54E+03
0.2214	1.69E+07	0.3438	5.07E+05	1.5536	1.06E+03
0.2266	1.60E+03	0.3459	6.42E+06	1.7378	2.40E+03
0.2272	1.49E+03	0.3501	2.52E+03	1.7657	1.03E+03
0.2288	1.35E+06	0.3518	1.18E+04	1.8317	1.89E+03
0.2335	6.76E+06	0.3561	8.45E+05		
0.236	1.56E+06	0.3573	1.10E+03		
0.236	2.28E+03	0.3879	6.42E+06		
0.2402	4.73E+04	0.3903	6.76E+06		

Table 21: Line energy spectrum of uranium-235 above 0.12 MeV